La investigación reportada en esta tesis es parte de los programas de investigación del CICESE (Centro de Investigación Científica y de Educación Superior de Ensenada, Baja California).

La investigación fue financiada por el SECIHTI (Secretaría de Ciencia, Humanidades, Tecnología e Innovación).

Centro de Investigación Científica y de Educación Superior de Ensenada, Baja California

Master in science
in Life science

Analysis and characterization of the diversity of viral particles of the vine mealybug (*Planococcus ficus* Signoret 1875) in the vineyards of Baja California

A dissertation
submitted in partial satisfaction of the requirements for the degree
Master in science

By:

Marco Antonio Cisneros Vargas

Ensenada, Baja California, México
2025

A Dissertation Presented by

Marco Antonio Cisneros Vargas

And approved by the following Committee

Dr. Jimena Carillo Tripp
Thesis codirector

Dr. Miguel Ángel Martínez Mercado
Thesis codirector

Dr. Roberto Cruz Flores

Dr. Rubén Darío Cadena Nava

Dr. Edgardo Alfredo Sepúlveda Sánchez Hidalgo
Postgraduate Coordinator in Life Sciences

Dr. Ana Denise Re Araujo
Director of Graduate Studies

Resumen de la tesis que presenta Marco Antonio Cisneros Vargas como requisito parcial para la obtención del grado de Maestría en Ciencias de la vida.

Análisis y caracterización de la diversidad de partículas virales del piojo harinoso de la vid (*Planococcus ficus* Signoret 1875) en los viñedos de Baja California

Resumen aprobado por:

Dra. Jimena Carrillo Tripp
Codirectora

Dr. Miguel Ángel Martínez Mercado
Codirector

La viticultura en Baja California es económicamente significativa, pero enfrenta desafíos como las infestaciones del piojo harinoso de la vid (PHV; *Planococcus ficus* Signoret). Esta plaga daña las vides al alimentarse de la savia, excretar melaza que provoca el crecimiento de fumagina y transmitir virus de plantas, lo que reduce la calidad y el rendimiento de las uvas. Investigaciones previas han revelado una gran diversidad de secuencias virales asociadas con el PHV, incluidas cinco nuevas secuencias de genomas virales de ARN pertenecientes a las familias *Iflaviridae*, *Dicistroviridae*, *Reoviridae* y *Tombusviridae*. Sin embargo, aún no se dispone de evidencia visual que confirme la presencia de partículas con morfología similar a las de estas familias virales. Este estudio tiene como objetivo caracterizar las partículas virales asociadas al PHV. Se recolectaron ejemplares de viñedos en el Valle de Guadalupe, Ensenada, y se procesaron para enriquecimiento de partículas virales. El enriquecimiento fue llevado a cabo mediante extracción, concentración y separación, y las suspensiones obtenidas fueron visualizadas utilizando microscopía electrónica de transmisión (TEM). Las imágenes de TEM se procesaron para contar y medir las partículas virales, creando un catálogo detallado de 259 partículas observadas. Las coincidencias en tamaño y morfología con familias virales conocidas incluyeron *Iflaviridae* (30-35 nm), *Dicistroviridae* (30-40 nm), *Reoviridae* (60-90 nm), *Tombusviridae* (28-34 nm) y partículas del orden *Picornavirales* (30 nm). Además, algunas partículas no coincidieron con los virus asociados previamente reportados en PHV, lo que sugiere la posibilidad de nuevos registros de virus. Estos hallazgos profundizan nuestra comprensión del viroma del PHV y confirman la existencia de partículas virales correspondientes a los genomas virales previamente reportados. Estudios adicionales, incluidos bioensayos, para los cuales se estandarizaron las metodologías durante este trabajo, ayudarán a probar su infectividad y su potencial uso en la gestión de poblaciones de PHV.

Palabras clave: Partículas virales, partículas tipo virus, piojo harinoso de la vid, ultracentrifugación y microscopía electrónica de transmisión

Abstract of the thesis presented by Marco Antonio Cisneros Vargas as a partial requirement to obtain the Master in science degree in Life science

Analysis and characterization of the diversity of viral particles of the vine mealybug (*Planococcus ficus* Signoret 1875) in the vineyards of Baja California

Abstract approved by:

Dr. Jimena Carrillo Tripp
Codirector

Dr. Miguel Ángel Martínez Mercado
Codirector

Viticulture in Baja California is economically significant but faces challenges such as infestations of the vine mealybug (*Planococcus ficus* Signoret). This pest damages vines by feeding on sap, excreting honeydew that promotes the growth of sooty mold, and transmitting plant viruses, which reduce the quality and yield of grapes. Previous research has revealed a great diversity of viral sequences associated with the vine mealybug, including five new RNA virus genome sequences belonging to the families *Iflaviridae*, *Dicistroviridae*, *Reoviridae*, and *Tombusviridae*. However, there is still no visual evidence confirming the presence of particles morphologically similar to these viral families. This study aims to characterize the viral particles associated with the vine mealybug. Mealybugs were collected from vineyards in the Valle de Guadalupe, Ensenada, and processed for viral particle enrichment. The enrichment was performed through extraction, concentration, and separation, and the resulting suspensions were visualized using transmission electron microscopy (TEM). TEM images were processed to count and measure viral particles, creating a detailed catalog of 259 observed particles. Size and morphology match with known viral families included *Iflaviridae* (30–35 nm), *Dicistroviridae* (30–40 nm), *Reoviridae* (60–90 nm), *Tombusviridae* (28–34 nm), and particles from the order *Picornavirales* (30 nm). Additionally, some particles did not match previously reported viruses associated with vine mealybugs, suggesting the possible presence non reported viruses. These findings deepen our understanding of the vine mealybug virome and confirm the existence of viral particles corresponding to previously reported viral genomes. Further studies, including bioassays standardized during this work, will help test their infectivity and potential use in managing vine mealybug populations.

Keywords: Viral particles, viral-like particles, vine mealybug, ultracentrifugation, and transmission electron microscopy

Dedication

A mis padres, María Guadalupe Vargas y José Antonio Cisneros Rodríguez

Por motivarme y apoyarme a retomar mis estudios después de haberlos interrumpido. Gracias a su respaldo, pude vivir esta experiencia increíble.

Acknowledgements

I extend my deepest gratitude to SECIHTI (Secretaría de Ciencia, Humanidades, Tecnología e Innovación) for the scholarship that supported me throughout my master's studies. This assistance was invaluable to my academic journey.

I am also thankful to CICESE (Centro de Investigación Científica y de Educación Superior de Ensenada, Baja California) and the Department of Microbiology for the knowledge and inspiration gained from its dedicated staff, whose passion for science motivates me to continue striving forward.

A special acknowledgment goes to Dr. Bernardino Ricardo Eaton González for the valuable lessons during my university years and for being an inspiring mentor who motivated me to pursue a master's degree. Your influence has left a lasting mark on my path.

To Dr. Jimena Carrillo Tripp, thank you for welcoming me into your lab. This period has been the most enriching phase of my life, deepening my understanding of virology and reinforcing my passion for this field. While I may not have been your top student, your guidance has inspired me to keep pushing forward and strive for excellence. Your patience and unwavering support have had an invaluable impact on my journey, and I am truly grateful for everything you have taught me.

To Dr. Miguel Ángel Martínez Mercado, thank you for co-directing my thesis. Your dedication and methodical approach to your work have inspired me greatly. Alongside Dr. Jimena, you set a standard that I strive to reach. I hope that one day, I will be confident enough in my work to consider myself a true colleague.

I extend my thanks to El Departamento de Biotecnología Marina, especially Dr. Clara Galindo and Dr. Edna Sánchez Castrejón, for allowing me to use some of their equipment.

To Dr. Rosa and Dr. Diego, thank you for lending me the stereoscope used in this project.

I also acknowledge the Comité Estatal de Sanidad Vegetal de Baja California (CESVBC) and Gaby Moyano for granting us access to the 11 sites used for recollections, providing transportation, and sharing invaluable teachings about the behavior of vine mealybugs.

I am deeply grateful to Dr. David Schneider and his university students for their invaluable help as volunteers during the recollection phase, as well as for the insights provided by Dr. Schneider on the behavior of mealybugs.

To my lab mates in Virolab Karen, Daylin, Cynthia, and Idalia thank you for your feedback and our thought provoking conversations. These moments opened my mind to new perspectives. I also acknowledge the students who completed their service activities, especially Yael Mijangos Limeta, whose eagerness to learn and significant help measuring particles underscored your bright potential.

Contents

List of figures

List of tables

Chapter 1. Introduction

In 2021, wine producers in Baja California's Valle de Guadalupe generated an estimated 595 million pesos in economic impact through the commercialization of approximately 22,800 tons of fruit (Secretaría de Agricultura y Desarrollo Rural, 2022). Beyond direct sales, grape cultivation plays a central role in Ensenada's economy, supporting a thriving tourism sector. According to projections by El Economista, the 2024 Grape Harvest Festival (Fiestas de la Vendimia) is expected to generate 800 million pesos, underscoring the broader economic significance of the region's grape industry.

Despite its ideal climatic conditions, Baja California's grape production faces several challenges. Water scarcity remains a primary constraint, particularly in Valle de Guadalupe, where limited water availability affects vineyard productivity (González Andrade, 2015). In addition to hydrological limitations, reliance on monoculture creates favorable conditions for insect pest outbreaks (Liu et al., 2018). Among these pests, the vine mealybug *(Planococcus ficus*) is one of the most significant threats to wine production, posing risks to both yield and quality (Cocco et al., 2021).

1.1 Background

Duarte de Jesús (2020) conducted the first virological study on the vine mealybug within the CICESE research group, identifying viral sequences associated with this pest through bioinformatics analysis. His findings provided a foundation for subsequent investigations, including Delgado Silva (2022), who characterized plant viruses carried by the vine mealybug in Baja California, and Cerezo Limón (2022), who analyzed the genome of one of the viruses found in vine mealybugs (Planococcus ficus-associated reovirus 1; PfRV1). Together, these studies established an initial framework for understanding the vine mealybug virome and its potential implications for viticulture.

Building on this foundation, the present study shifts the focus from sequence-based to the direct identification and morphological characterization of viral particles associated with vine mealybug. While Duarte de Jesús (2020) initiated efforts to enrich virus-like particles (VLPs) to characterize virus morphology to support his bioinformatics findings, this study refines and standardizes isolation methodologies to improve VLP recovery and analysis by establishing a methodological approach, that aims

to bridge the gap between genomic data and physical evidence, improving the isolation of VLPs to aid in identification of viral entities present in the vine mealybug.

1.2 The vine mealybug

Grapevines were introduced to Mexico in the 16th century by ecclesiastical institutions of Spanish origin (Wine Folly, 2024). However, the vine mealybug (*Planococcus ficus*) was not recorded in Mexico until 2000, when it was first identified in Hermosillo, Sonora (Gobierno de México, 2022). Its presence was later confirmed in vineyards in Ensenada, Baja California, in 2014, highlighting its recent establishment in key viticultural regions (Gobierno de México, 2022).

The vine mealybug belongs to the family Pseudococcidae within the order Hemiptera (Walton & Pringle, 2004). Adult females measure approximately 4 mm in length, 2 mm in width, and 1.5 mm in height, and are covered in a fragile, waxy secretion (Waterworth et al., 2011). Males are smaller, possess segmented bodies, lack oral apparatus, and are equipped with wings and anal filaments, adaptations that facilitate dispersal (Walton & Pringle, 2003) (Figure 1).

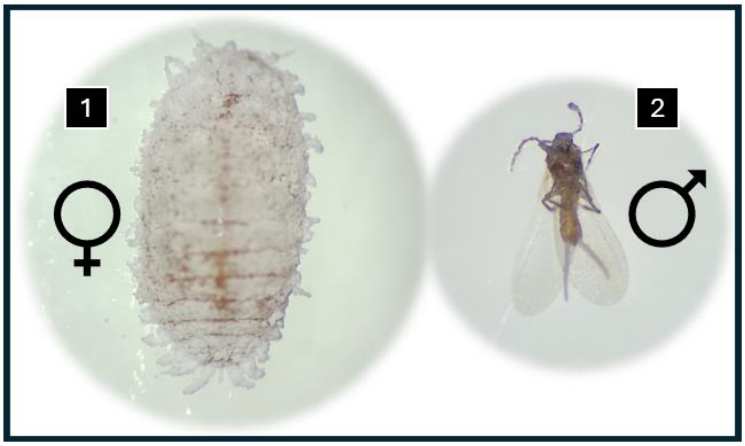

Figure 1. Vine mealybug sexual dimorphism. (1) Adult female vine mealybug (fourth instar) 4 mm length and 1.5 mm width. (2) Adult male vine mealybug 2 mm length.

Vine mealybugs reach sexual maturity approximately 31 days after hatching for both males and females (Walton & Pringle, 2004). Females lay an average of 362 eggs per ovisac, though more recent studies suggest a broader range of 300 to 700 eggs per ovisac (Waterworth et al., 2011). Populations typically undergo up to six generations per year, though environmental factors can influence the frequency of

generations (Walton & Pringle, 2004). Cocco et al. (2021) noted that various stressors, including resource availability and climatic conditions, may accelerate generational cycles. Among these factors, temperature is the primary driver, as higher temperatures have been linked to increased egg production and a greater number of annual generations (Walton & Pringle, 2004) (Figure 2).

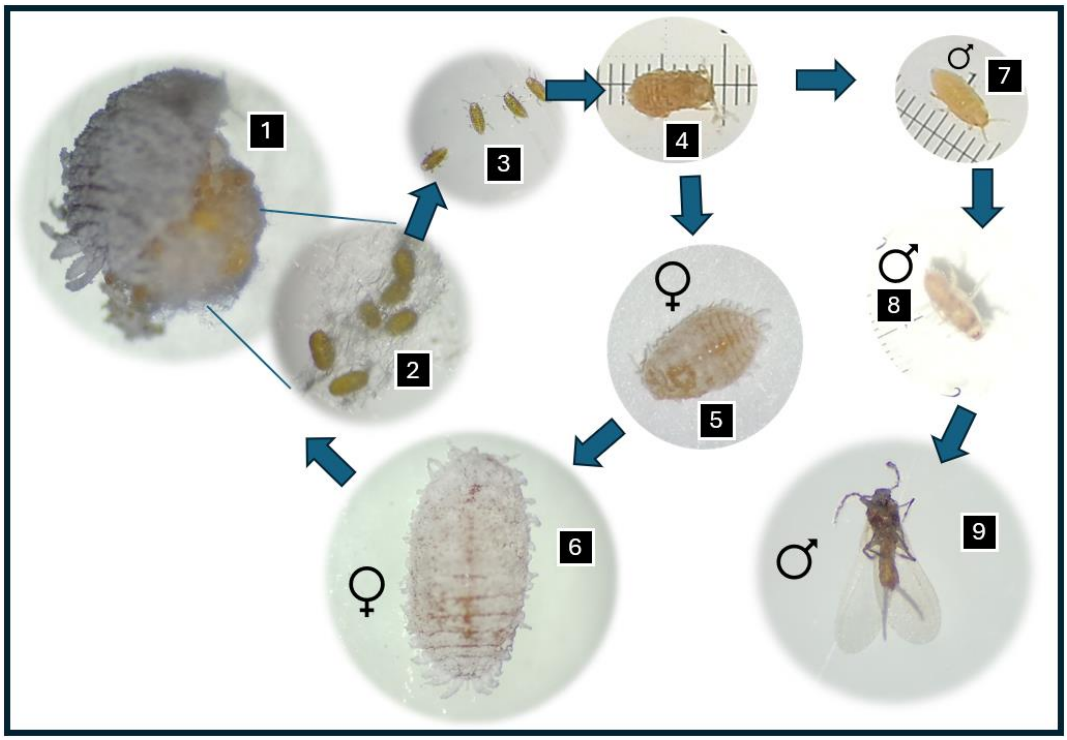

Figure 2. Vine mealybug life cycle. (1) Adult female vine mealybug with an egg sack. (2) Close up picture of eggs sack. (3) Newborn crawlers (First instar). (4) Second instar mealybug (Image credit: Tonya Ivette Delgado Silva). (5) Female nymph (Third instar). (6) Adult female mealybug (Fourth instar). (7) Male prepupa (Image credit: Tonya Ivette Delgado Silva). (8) Male pupa. (9) Adult male mealybug.

1.3 Impact of vine mealybug on grapevine cultivation

The vine mealybug is a significant pest in the wine industry, causing substantial damage to grapevines and reducing yield through direct and indirect mechanisms. Feeding on the plant's phloem places considerable physiological stress on the vine, while the excretion of honeydew promotes the growth of sooty mold, leading to trunk discoloration and a decline in fruit quality. Beyond these effects, the vine mealybug serves as a vector for several viruses, including those responsible for grapevine leafroll disease, one of the most economically damaging grapevine diseases, capable of reducing yield by 30% to 50% (Atallah et al., 2012).

Population dynamics of the vine mealybug fluctuate seasonally, with significant increases observed in August and September, coinciding with rising temperatures. This period aligns with key grapevine phenological stages, such as maturation and ripening, when pest pressure is particularly problematic. Field studies have reported noticeable population peaks during these months (Solaiman et al, 2020), posing challenges for vineyard management. The proximity of these peaks to the harvest season further complicates control efforts, as regulatory restrictions limit the application of chemical treatments near harvest.

1.4 Virome

An organism's virome encompasses all viral entities associated with it, including viruses that directly infect the host and those interacting with its microbiome. As an example, in the case of eukaryotes these would include eukaryotic viruses, which may cause chronic or acute infections, and bacteriophages, which regulate bacterial and archaeal communities within the microbiome. Additionally, virus-derived genetic elements integrated into the host genome can influence gene expression and immune responses (Virgin, 2014). Through these interactions, viromes contribute to host fitness by modulating microbiome composition, immune function, and other physiological processes (Handley, 2016).

Insects represent an ideal model for virome studies due to their diverse viral populations and distinct antiviral mechanisms, such as RNA interference (RNAi), which plays a crucial role in limiting viral infections. Insect viromes provide insight into host-virus co-evolution, revealing how viral diversity and host adaptability are shaped over time (van Mierlo et al., 2014).

Characterizing an organism’s virome requires multiple levels of validation beyond sequence identification. While genomic data offers insights into evolutionary relationships and potential viral associations, experimental confirmation is necessary to distinguish actual viruses from virus-derived sequences. For the study of insects virome this process includes closing sequence gaps to assemble complete viral genomes, detecting replication markers (e.g., dsRNA detection for RNA viruses or small RNA sequencing), visualizing viral particles via electron microscopy, and isolating functional viral entities for infectivity assays in host insects or cell cultures (Bonning, 2020). Each of these steps strengthens the link between sequence data and functional virological evidence.

In this context, VLPs serve as a crucial component of integrative virome studies. In virology it refers to particles resembling virions that require further analysis to confirm their classification. However, in biotechnology, VLPs are non-infectious protein structures that mimic viral particle morphology (Meulenberg & Petersen-den Besten, 1996).

1.5 Primary methods used for the morphological characterization of viruses

The classification of viral particles relies on multiple characteristics, including the presence or absence of an envelope, dimensions, density, and genome type. These parameters are fundamental to the taxonomic framework established by the International Committee on Taxonomy of Viruses (ICTV)(Walker et al., 2022; Zhao et al., 2021). Accurately determining these features requires an integrative approach that combines molecular techniques and microscopy (Richert-Pöggeler et al., 2018).

Among microscopy techniques, transmission electron microscopy (TEM) and scanning electron microscopy (SEM) are widely used for viral structure visualization. TEM provides high-resolution imaging of internal viral architecture, while SEM enables the examination of surface morphology and topographical details (Qin et al., 2019; Hammond et al., 1981; Katz & Kohn, 1984).

In addition to SEM and TEM, atomic force microscopy (AFM) enables the study of virus-host interactions at the nanoscale under near-physiological conditions, offering insights into structural changes and binding mechanisms (Mateu, 2012). Cryo-TEM, with its ability to capture virus particles in a near-native state, is particularly valuable for studying virus assembly, protein interactions, and 3D reconstructions of viral capsid architecture. This technique provides unparalleled structural detail but is costly and less accessible for routine use (Yu et al., 2007).

To obtain purified viral particles for characterization, ultracentrifugation combined with density gradient separation is a widely used approach. Sucrose or cesium chloride gradients allow for the isolation and concentration of VLPs based on size, density, and structural properties (Miyamoto et al., 1992; Nasukawa et al., 2017). This method enables the recovery of both enveloped and non-enveloped virus particles, facilitating their subsequent classification through electron microscopy and molecular techniques (Roingeard, 2008). Proper isolation and purification ensure that the collected samples are free of contaminants, enhancing the accuracy of viral morphology studies.

Accurate viral classification requires analyzing distinct structural features, including capsid architecture, size, and buoyant density. For instance, members of *Iflaviridae* and *Dicistroviridae*, both within the order *Picornavirales*, exhibit small icosahedral virions (~30 nm in diameter) but differ slightly in buoyancy density. Iflaviruses have a density range of 1.29–1.38 g/cm³, whereas dicistroviruses range from 1.34–1.39 g/cm³ in cesium chloride gradients (Bonning & Miller, 2010; Zell et al., 2017).

In contrast, the virions of reovirus are significantly larger (60–90 nm in diameter) and are characterized by multi-layered capsids, distinguishing them from the single-layered capsids of picornaviruses such as iflaviruses and dicistroviruses (ICTV, 2022). The differences in size and density among these particles play a crucial role in ultracentrifugation-based separation, where gradient techniques allow for the isolation of smaller, single-layered virions from larger, multi-layered capsids. This comparison highlights how size, structural complexity, and density influence VLP classification and separation, aiding in the identification of viral entities.

This study builds upon the findings of Duarte de Jesús (2020), who identified RNA and DNA viral sequences associated with the vine mealybug. While previous research focused on sequencing-based detection, this study emphasizes VLP characterization, with particular attention to viral families previously documented in arthropods, as some of these viruses may hold potential for use as biocontrol agents.

1.6 Justification

The vine mealybug is a significant pest in viticulture, yet its virome remains largely uncharacterized. This study seeks to advance current knowledge by visualizing and characterizing VLPs associated with this insect. By focusing on morphological analysis and structural characterization, this work aims to provide a more comprehensive understanding of viral diversity within the vine mealybug. Identifying and classifying these viral entities may reveal entomopathogenic viruses with potential applications in biological control strategies.

1.7 Hypothesis

The vine mealybug harbors VLPs with morphologies consistent with multiple viral families, including *Dicistroviridae*, *Tymoviridae*, *Reoviridae*, *Rhabdoviridae*, *Tombusviridae*, and *Iflaviridae*, as well as potential non reported viruses.

1.8 Objectives

1.8.1 Main objective

Characterize viral particles associated with vine mealybugs from Ensenada, Baja California.

1.8.2 Specific objectives

1. To analyze the morphological properties of viral particles isolated from vine mealybugs.

2. To establish and optimize the protocols and methodology to test the infectivity of viral particles in vine mealybugs

Chapter 2. Methodology

2.1 Field collection of vine mealybugs

A total of thirteen field trips to 11 sites were organized in collaboration with the State Committee for Plant Health of Baja California (CESVBC). The committee provided training and guidance on collecting vine mealybugs and facilitated access to vineyards through connections with grape producers in the Valle de Guadalupe, Ensenada, Baja California (Figure 3), the recollection period took place from January 2023 to August 2023. To respect the privacy of the landowners, the specific names of the collection sites are not disclosed.

Figure 3. Recollection sites. (1) Satellite images of Valle de Guadalupe, Baja California, showing recollection sites from eleven vineyards. Vine mealybugs from the red marked sites yielded the highest biomass. Image modified from Google Earth. (2) Satellite image of Baja California, with the recollection region of Valle de Guadalupe indicated by a red marker. Image modified from Google Earth.

Key indicators were used to identify potentially infected grapevines, such as the presence of ants, a darkened trunk crust from mealybug excretions, and cotton-like structures left by the vine mealybugs. These factors reliably indicated mealybug infestations (Figure 4).

The collection process was carried out either manually using a fine brush and 50 mL Falcon tube or with the assistance of a portable vacuum unit (Alkesi). Infected vines were inspected, and vine mealybugs were collected from various plant parts, including trunks, arms, and roots, depending on the phenological stage

of the grapevine. Collected vine mealybugs were immediately stored in iceboxes at 4°C to preserve their integrity during transport to the laboratory.

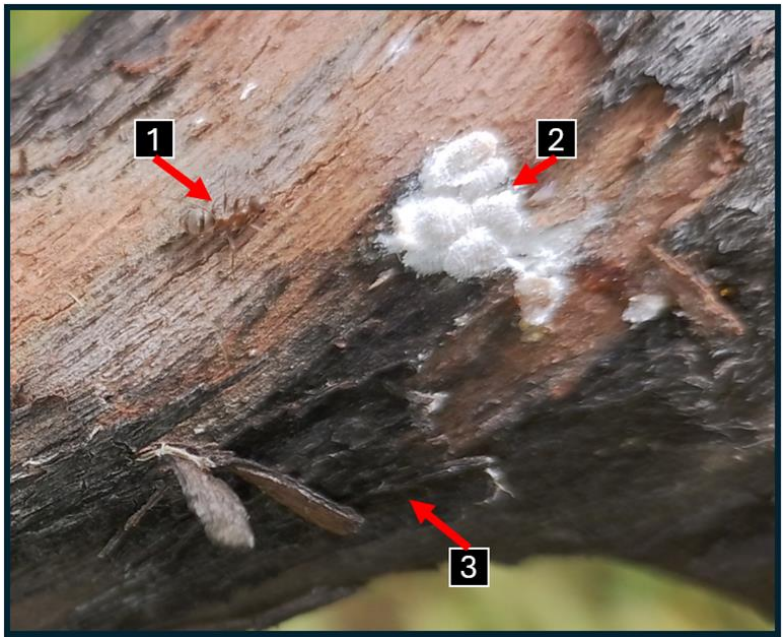

Figure 4. Key indicators of vine mealybug presence. (1) Presence of ants. (2) Group of vine mealybugs with a cotton-like structure. (3) Darkened crust in the grapevine bark.

Upon arrival at the lab, the vine mealybugs were stored at 4°C until further processing. Cleaning of the samples involved using a stereoscope to separate vine mealybugs from additional materials like ants and wood chips (Figure 5). Typically, the cleaning process occurred the day after collection. Once cleaned, the vine mealybugs were weighed to determine collected biomass and stored at 4°C. Vine mealybug samples had to be cleaned within 24 hours to allow storage at -20°C.

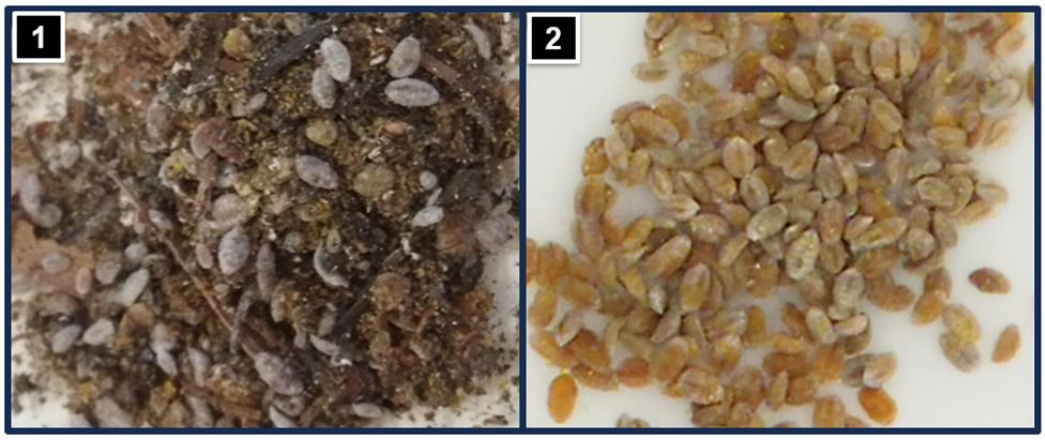

Figure 5. Mealybug cleaning process. (1) Vine mealybugs before stereoscope cleaning. (2) Vine mealybugs after stereoscope cleaning. Photos by Jimena Carrillo Tripp.

2.2 Mass rearing of vine mealybugs

A vine mealybug colony was initiated using adult females from five selected collection sites (S1, S2, S4, S5, S10) (Figure 3) and maintained throughout the study. Twenty adult females were selected per site and placed in jars containing sprouted Russet potatoes, serving as a food source and support structure (Mani & Shivaraju, 2016). The jars were covered with a 0.11-mm caliber filter mesh to prevent the vine mealybugs from escaping while enabling air circulation (Figure 6).

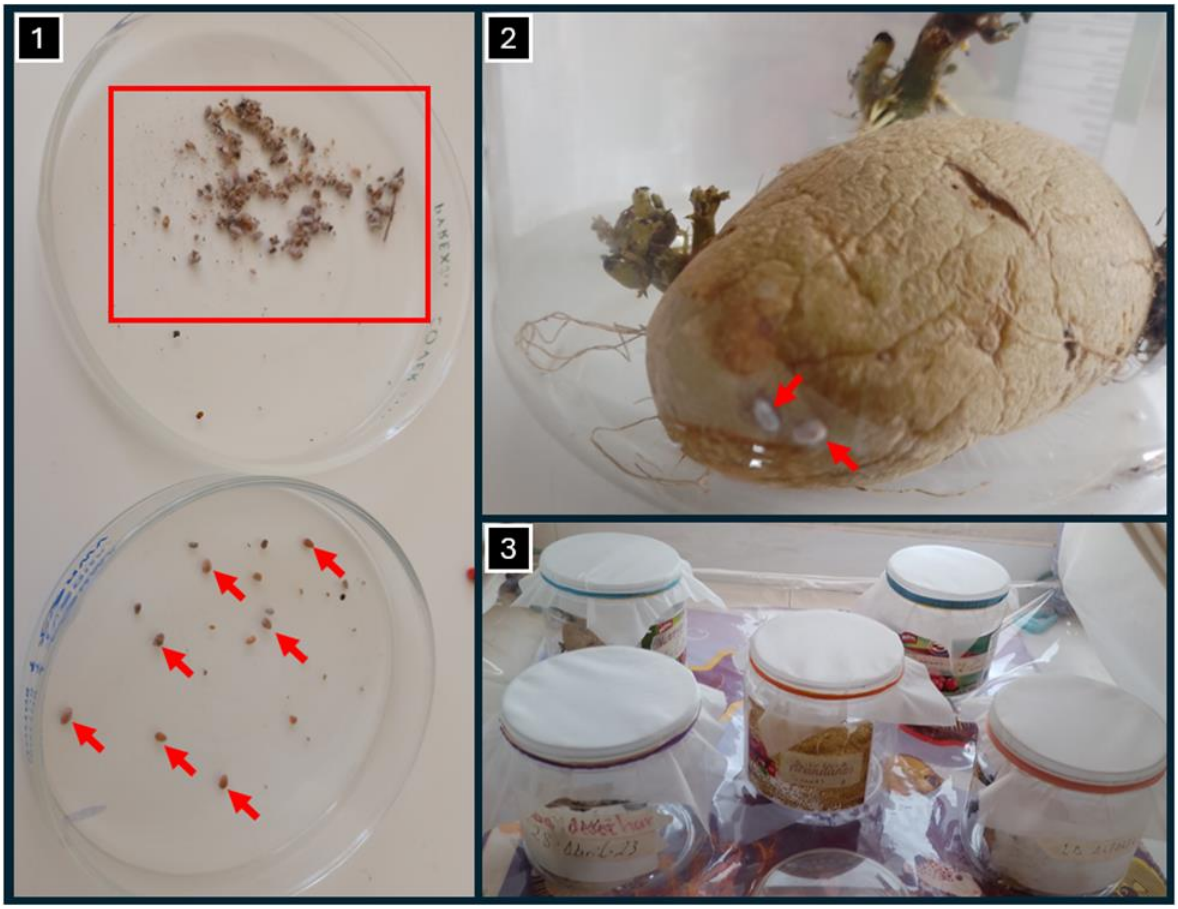

Figure 6. Selection of founding females. (1) Material before screening and cleaning (red box), selection of founders (red arrows). (2) Breeding stock with adult vine mealybugs starting oviposition (red arrows). (3) Five breeding stocks.

Temperature was maintained between 27°C and 29°C using seedling heating mats (Seed Factor), with relative humidity between 60% and 80%, regulated through ventilation. Temperature and humidity were monitored using a datalogger (Elitech RC-51H PDF USB). Colonies were inspected every two days, with potatoes being replaced monthly to ensure a continuous food supply.

To support the colony, medium-sized Russet potatoes were stored at 2.2°C for 1–2 months before sprouting. Sprouted potatoes were planted in pots filled with Cosmopeat and covered with slightly damp soil under control conditions. To provide immediate sustenance, additional sprouted potatoes (3–5 cm sprouts) were placed on top of the soil (Figure 7). Meanwhile, another batch of potatoes was planted and grown in a greenhouse, away from vine mealybugs, until their sprouts reached 20–30 cm. These were inspected for foreign insects before being introduced to the colony to maintain food quality and availability.

Figure 7. Vine mealybugs sustain. (1) Potato sprouts introduced to the vine mealybug colony. (2) Potatoes over the soil for immediate sustainment.

The breeding stock colony successfully generated multiple generations (Figure 8). Monitoring every two days ensured colony stability and health. The colony served as a consistent source of vine mealybugs for protocol optimization and experimental studies, including eclosion characterization, testing of transmembrane feeders (ATM) effectiveness, and infectivity assay. The colony establishment period spanned from January 24 to August 31, 2023, providing a robust foundation for experimental investigations.

Figure 8. Mealybug breeding stock. (1) Breeding stock first generation of crawlers (red arrows). (2) Breeding stock third generation of adult vine mealybugs.

2.3 Viral particle extraction and concentration

The viral particle extraction and concentration processes were adapted from the protocols by Luria et al. (2020) and Feng et al. (2017). Feng's protocol was incorporated because it was successfully used by Duarte de Jesús (2020). Luria's protocol, applied to the closely related mealybug species *Phenacoccus solenopsis*, provided additional context for VLP extraction. In this study, vine mealybugs were cleaned, macerated, and processed for viral particle recovery (for full methodology, see Annex 1).

One gram of vine mealybugs was macerated with 6 mL of a buffer solution consisting of TBE (Tris/Borate/EDTA) and PB (Phosphate Buffer) at a 1:1 ratio (v/v). The macerate was then distributed into 4 Eppendorf tubes and centrifuged at 14,000 x g for 10 minutes at 4°C using a Hermle centrifuge (z 216 mk). The supernatant (S1) was collected in a 15 mL tube, while the pellet (P1) was retained. 600 µL TBE buffer and 60 µL chloroform: n-butanol (1:1 v/v) were added to P1, vortexed, and centrifuged again using the same parameters (14,000 x g for 10 minutes at 4°C). Supernatant (S2) was collected (Figure 12). Both S1 and S2 were filtered, with S1 being filtered through a 0.8 µm hydrophilic mixed cellulose ester (MCE) membrane followed by a 0.45 µm polyethersulfone (PES) filter, and S2 through a 0.45 µm PES filter (Figure 9).

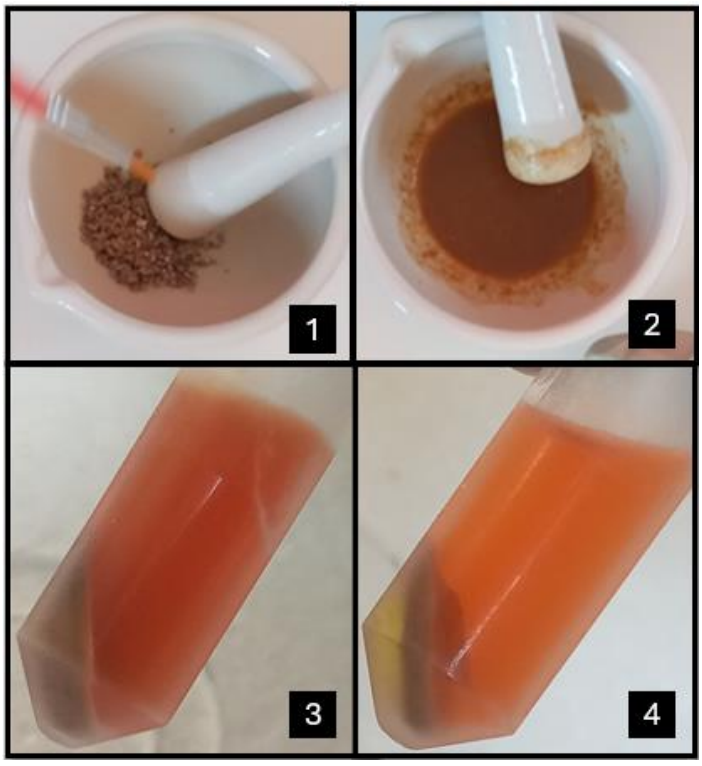

Figure 9. Viral particle extraction initial steps. (1) Adult mealybug. (2) Macerated vine mealybugs. (3) Supernatant (S1). (4) Supernatant (S2).

S1 and S2 filtrates were placed into labeled polypropylene centrifuge tubes (5 mL, Open-Top Thinwall Polypropylene Tube, 13 x 51 mm Millex) and ultracentrifuged at 160,000 x g for 3 hours at 4°C. After ultracentrifugation (Beckerman Optima Max XP ultracentrifuge, MLS-50 swing bucket rotor), the supernatants were discarded, and a 0.5 mL PB buffer was added to each tube. The tubes were sealed with parafilm and stored overnight at 4°C (Figure 10).

Figure 10. VLP concentration. (1) The Optima Max XP ultracentrifuge (Beckman). (2) Pellets formed after ultracentrifugation.

2.4 Sucrose gradient separation and sample cleaning

The pellets resulting from S1 and S2 concentration were resuspended in 1.5 mL of PB buffer each, resulting in a total volume of 3 mL. Each of these 3 mL resuspensions (S1 and S2) were then divided into two equal portions of 1.5 mL to be used for the gradient separation.

A sucrose gradient was prepared in 5 mL, Open-Top Thinwall Ultra-Clear Beckman tubes (13 x 51 mm), by sequentially adding seven steps of 0.5 mL sucrose/PB solution, with sucrose concentrations of 10%, 15%, 20%, 25%, 30%, 35%, and 40%, starting from the lowest concentration (10%) to the highest (40%), the gradient preparation was done in a cold room at 4°C. After preparing the gradient, 1.5 mL of the resuspended pellet (either from S1 or S2) was carefully layered on top of the sucrose gradient, making the

total volume in each tube 5 mL (3.5 mL from the sucrose gradient and 1.5 mL of resuspended pellet). The tubes were balanced with their corresponding pairs and ultracentrifuged at 100,000 x g for 2 hours at 4°C.

After centrifugation, the gradient was fractionated into three parts. The top fraction was recovered first, by carefully removing the liquid from the meniscus, without targeting a specific volume, but rather until reaching the area just above the resulting visible band. This ensured that the next fraction would contain the visible band accurately.

The second fraction, containing the band, was then collected and the remaining volume was recovered as the third fraction, including the bottom of the tube. If a pellet was present at the bottom, it was resuspended with the remaining liquid from the third fraction.

Once the gradients were divided into three fractions (top, band-containing, and bottom), the fractions were consolidated, the top and bottom fractions were merged, while the band containing fraction remained separate.

2.5 Sucrose cleaning

Excess sucrose was removed from samples in the following way. PB buffer was added to each sample (top and bottom consolidated, and the band) from each origin (S1 and S2) until the total volume reached 20 mL. Each of these suspensions were ultracentrifuged at 200,000 x g for 2 hours at 4°C, and the supernatants were discarded.

For each of the suspensions S1 and S2, this process yielded 8 pellets: 4 from the combined top and bottom fractions and 4 from the band fraction. Each pellet was resuspended in 50 µL of PB buffer. The resuspended pellets from the top and bottom fractions were combined, resulting in a 200 µL suspension, while the pellets from the band fractions were similarly combined to form another 200 µL suspension. All suspensions were stored at 4°C until further use.

2.6 TEM sample preparation and imaging

Samples for TEM microscopy were carefully resuspended with a micropipette to ensure a uniform suspension and prevent any sedimentation of material. A 10 µL droplet was placed on a copper grid (Ted

Pella Athene 400 Mesh Grid) following the sample mounting process used for negative stain TEM (Laboratorio Nacional de Microscopía Avanzada CICESE, LNMA), the droplet was left for 2 minutes before being absorbed with absorbent paper without touching the grid. A 10 µL droplet of 2% uranyl acetate was then added to the grid and incubated for 3 minutes. The droplet was removed using absorbent paper, and the grid was dried under a 60 W incandescent light bulb for 30 minutes at 30 cm. This procedure follows common methodologies for negative stain TEM, such as those described by Tizro (2019), with the main modification being the drying step under the light bulb. The samples were prepared 2 days prior to TEM microscopy. Mounted grids were stored in their cases and only removed for imaging. After imaging, they were returned to their cases.

TEM microscopy was conducted by an LNMA laboratory technician using a Hitachi 7500 electron microscope. The microscope was operated at a high tension (HT) of 80 kV. Magnification ranged from 100 KX to 25 KX, with lower magnifications used for panoramic overviews and higher magnifications applied to specific areas of interest where potential viral particles were observed. Images were captured from different quadrants of the grids.

Potential matches in size and morphology to particles from virus belonging to families such as *Iflaviridae* (30-35 nm), *Dicistroviridae* (30-40 nm), *Reoviridae* (60-80 nm), *Tombusviridae* (28-34 nm), and the order *Picornavirales* (30 nm) were referenced during analysis.

2.7 TEM images analysis

All TEM images were initially categorized into two groups: one containing potential viral particles and the other without them. The images without potential viral particles undergo further screening to assess methodological failures like the presence of any aberrations, the quantity of deposited material, and the occurrence of crystals (from sucrose or uranyl). These observations informed adjustments to the extraction, concentration, and separation protocols to optimize the methodology.

Images containing potential viral particles were subjected to detailed analysis. The morphology of the viral particles was carefully documented, including their shape, diameter, and length. These measurements were cross-referenced with known viral families and orders from previous works (Duarte de Jesús, 2020) and ICTV database. Viral particles were cataloged using ImageJ Fiji software. After initial screening and identification in the images, close-up captures were taken for measurement, with a reference scale added

to each. ImageJ was used to measure particle diameter or length, and all processed images were systematically stored.

The viral particles were categorized into two groups based on their morphology: group 1 (spherical/icosahedral particles) and group 2 (rodlike particles). A total of 159 spherical or icosahedral particles were measured from all the photographs taken of the sample suspensions for group 1.,. In contrast, for rod-like particles, due to their higher abundance, only 100 were measured to provide an accurate representation of their size range.

Histograms were generated to illustrate the distribution of VLP sizes observed across samples. To determine the optimal bin width and number of bins, the Freedman-Diaconis rule was applied, which considers data variability and sample size to enhance resolution while minimizing bias. The interquartile range (IQR) was calculated to measure data spread, and the bin width was defined as:

$$\boldsymbol{Bin\ width = 2xIQR \div \sqrt[3]{}}$$

where n represents the total number of VLP measurements. This approach ensured an accurate representation of size distributions without over-smoothing or artificially segmenting the data.

2.8 Transmembrane feeder design

The transmembrane feeder (ATM) was modified from the design specified by Arora et al. (2020) for the grape mealybug (*Pseudococcus maritimus*). A 15 mL Falcon tube was cut to a length of 3.5 cm with a diameter of 1.5 cm, using the side including the threads for the lid. The inner surface was sanded using 220-grade sandpaper. The lid was perforated at the center to create a 0.5 cm diameter hole (Figure 11).

A square piece of parafilm, measuring 2.5 cm per side, was stretched to approximately 7 cm to prevent the liquid diet from seeping through while creating a barrier akin to a plant's epidermis. This membrane served as a container for inoculation solutions and at the same time prevented the escape of the newborn crawlers from the top. The parafilm surface was roughened to provide texture without compromising its integrity and was then used to cover the open end of the tube (Figure 12). Additionally, two layers of coffee

filter paper were cut into circles and placed on the inner side of the perforated lid to prevent crawlers escaping the ATM's and permit airflow.

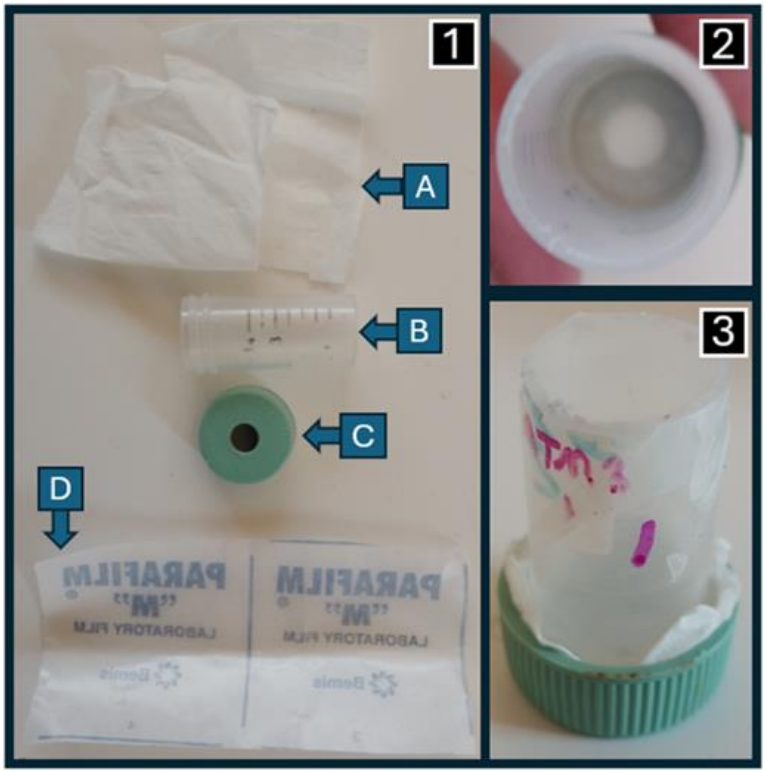

Figure 11. ATM set up. (1) (A) Coffee filter paper. (B) Modified 15 ml Falcon tube. (C) Perforated lid. (D) Parafilm sheet. (2) Assembled ATM without Parafilm membrane. (3) Fully assembled ATM.

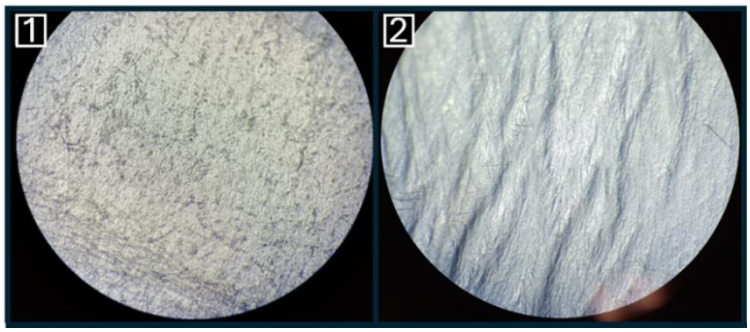

Figure 12. Detail of ATM parafilm membrane surface. (1) Unstretched parafilm membrane (smooth surface). (2) Stretched parafilm membrane (irregular surface).

2.9 Eclosion period characterization

The experiment involved 20 ATMs, with one ATM described here as a representative example. A female vine mealybug in its fourth instar (approximately 2 mm) was selected from the breeding stock colony,

examined under a stereoscope to ensure it was free from malformations, and transferred into the ATM using a fine brush. The ATM's top was sealed with a stretched membrane. Incubations proceeded at room temperature.

Observations were conducted daily between 12:00 and 15:00, with the bottom side of the ATM carefully opened to avoid disturbing the mealybug. Environmental temperature was recorded with a mercury thermometer, and oviposition was monitored. Oviposition was noted by the appearance of cotton-like structures under the progenitor, later containing amber-colored eggs. If detected, oviposition progress was tracked daily until crawlers (newborn vine mealybugs) emerged.

When crawlers were detected, the ATM was opened and positioned over a petri dish and gently flicked to collect the crawlers while avoiding dislodging the progenitor or disturbing the egg sac. Collected crawlers were registered and stored. This process continued daily until crawler production declined, indicating egg sac viability had ceased.

This procedure applied to each of the 20 ATMs, which were arranged in four sets of five replicates, with each set starting a day apart. The experiment spanned 21 days, during which all ATMs were monitored, and data on crawler emergence and environmental temperature was recorded to analyze the eclosion period and potential temperature influences.

2.10 ATM’s feeding effectiveness

Ten ATMs were set up, each containing a female vine mealybug at the fourth instar. The experiment was conducted following the methodology outlined in the eclosion experiment. One day prior to the anticipated peak of eclosion, 30 µL of buffer PB combined with 10 µL of food dye was applied on top of the stretched, irregular parafilm membrane. This was then covered with another parafilm membrane to secure the solution. Over the course of two days, crawlers were collected and categorized into dyed and undyed groups. The number of each type of crawler was recorded for further analysis (Figure 13).

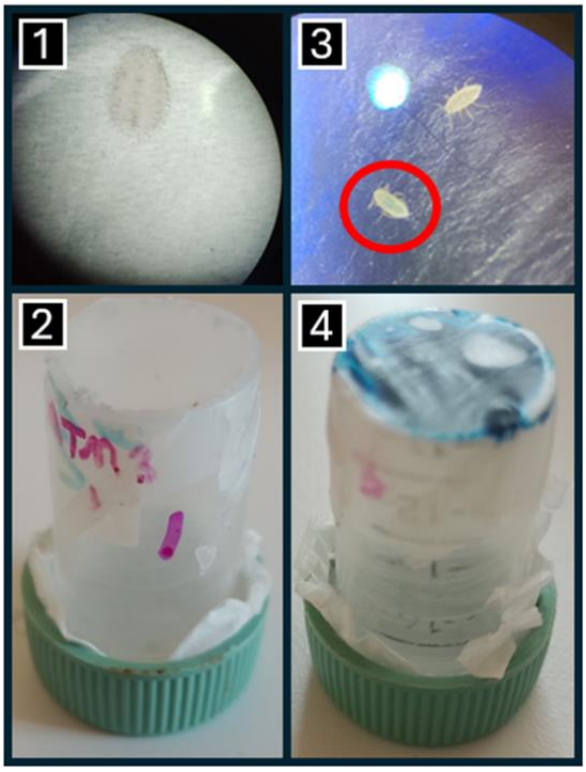

Figure 13. Feeding observation in ATM. (1) Adult vine mealybug (4th instar, progenitor). (2) ATM set up. (3) Newborn crawlers feed through the inner membrane, crawlers with dyed intestine visible (indicated by red circle). (4) ATM with dyed buffer.

2.11 Vine mealybug infectivity assay

This experiment was a preliminary attempt to establish a protocol for administering VLP treatments to vine mealybugs. The suspensions were prepared from S1 and S2 samples obtained from the enrichment protocol using material from the 11 recollection sites. These samples were visualized by TEM and confirmed to contain VLPs.

Each ATM was loaded with their respective treatment in 40 µL of solution: 30 µL of phosphate buffer (PB) with or without viral particles suspension and a dye mixture of 5 µL of blue food dye (Ma Baker and Chef) and 5 µL PB. For treatment A (TA) the concentration was a 1:1 mixture of VLP suspensions from both S1 and S2 fractionated bands plus 10 µL of dye mixture. Treatment B (TB) was a 1:10 of TA in PB plus 10 µL of dye mixture. The negative control (TC) consisted of 30 µL of PB and 10 µL of dye mixture.

Three ATMs per treatment was used to expose vine mealybug crawlers to VLPs or negative control. Three healthy fourth instar female mealybugs, were used for each ATM. ATMs were maintained at 27°C to 29°C

using a heating mat, with conditions monitored by a data logger. Six days after setup, each solution was applied, the treatment was replenished over five days if needed.

Treated mealybugs were visually examined daily under a stereo microscope, positive ones (identified by a blue dyed intestine) were transferred to potato-containing reservoirs for monitoring; meanwhile non-dyed crawlers were returned to their ATMs. Positive crawlers were categorized into three post-inoculation periods (PIs): PI1 included crawlers collected within two days and monitored for four days; PI2 included those collected over the following three days and monitored for an additional ten days. Survival rates were recorded for PI1 and PI2, and deaths were verified to ensure they were not due to mechanical damage, such as crushing by potatoes. PI3 included mealybugs and generated biomass collected after 130 days in their reservoir. For this case (PI3) the collected mealybugs and material were generated from the initially treated mealybugs.

Chapter 3. Results

3.1 Seasonal patterns in biomass collection

A total of 41.43 grams of mealybugs were collected over several months across 11 distinct sites. Biomass collection showed a clear seasonal pattern, with a gradual increase from 0.57 grams per trip in January to 1.05 grams in April, followed by fluctuations in May and June. The most significant collection rates were observed in the summer months, particularly in July (9.23 grams) and August (15.28 grams), indicating a peak in mealybug population during this period (Figure 14). The last two collection dates had a larger workforce of volunteers, especially the final collection, which involved 10 to 14 people, compared to the usual 4 to 5 people for earlier collections.

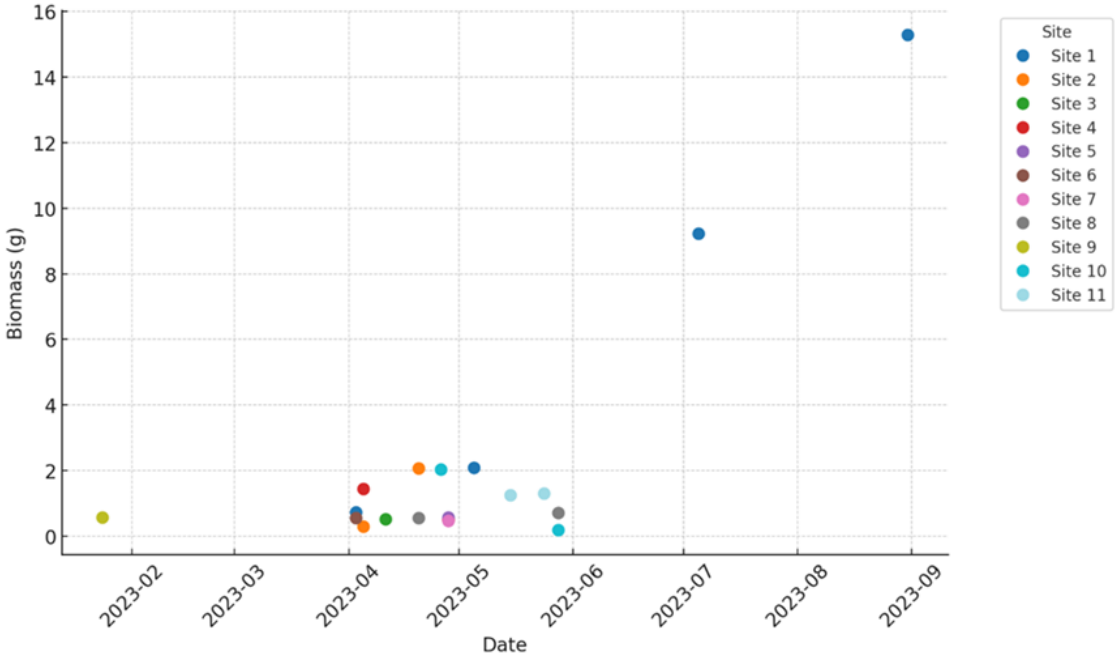

Figure 14. Mealybugs Collection. Scatter plot showing the collection dates and weight (in grams) for each site.

3.2 VLP enrichment protocol and characterization

The mealybugs used for VLP extraction and concentration protocols were from field sites: 1, 2, 4, 10, and 11 (Figure 3) to account for available biomass. Initially, Version 1 of the protocol followed the methodology outlined by Luria et al. (2020), which involved a single extraction with a buffer, producing only one

supernatant. Version 2 was developed to include a double extraction process, with the first extraction using buffer (yielding supernatant S1) and a second extraction using a chloroform:n-butanol mixture (1:1 v/v) on the pellet from S1 to produce supernatant S2 to further disrupt cellular membranes improving extraction on the possible remaining VLPs from the pellet generated after the first extraction. S1 supernatant consistently appeared denser with a milky texture, while S2 was clearer. Both supernatants initially showed a dark orange or amber color in early extractions (Figure 15).

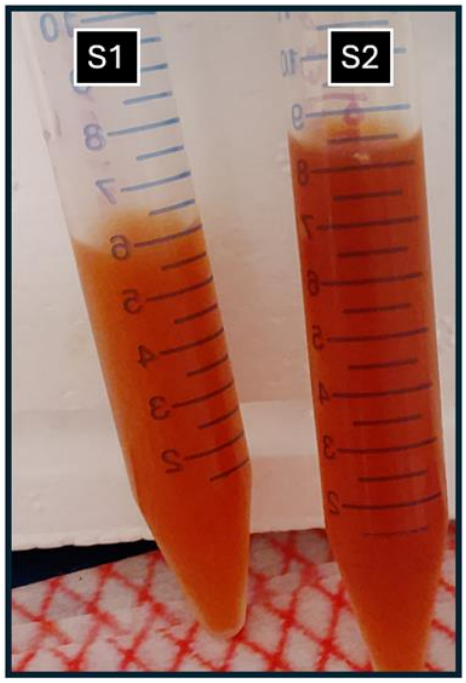

Figure 15. Extraction supernatants. (S1) Supernatant S1 after filtration, showing an amber color with a slight whitish tint. (S2) Supernatant S2, displaying a clearer, more translucent amber color.

As the protocol was refined, subsequent versions of the extraction process included mealybugs from all sites. Initially, enrichment runs were conducted using mealybugs from a subset of sites where greater biomass had been collected. Once the protocol was established, mealybugs from all sites were used in equal proportions, with 0.09 mg sourced from each site. During these later extractions, samples from site 6 displayed a darker brown color upon maceration, contrasting with the amber color typical of other sites (Figure 16). Individuals from site 6 were also more fragile, breaking easily during handling, and thawing faster under the same storage and processing conditions. Despite these site-specific variations, the overall distinctions between S1 and S2 remained consistent, with S1 retaining a milky appearance and S2 remaining clearer, even in the darker brown samples from site 6.

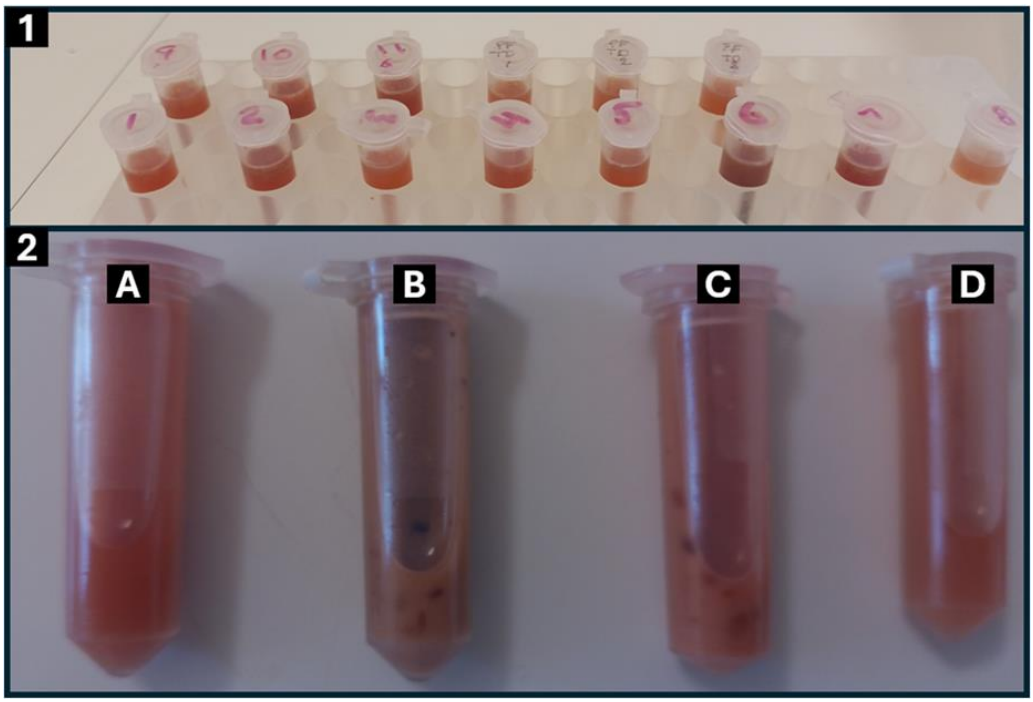

Figure 16. Macerated mealybugs by site. (1) Collection of macerated mealybugs of the 11 sites. (2) Comparison of sites 5 (A), 6 (B), 7 (C) and 8 (D).

The resulting pellets from each supernatant displayed distinct characteristics: S1 pellets were generally larger and darker in color, while S2 pellets were smaller and lighter, though both retained a brownish tint (Figure 17). These pellets then proceeded to sucrose gradient separation, revealing additional differences between the S1 and S2 material and providing insights into the composition of viral particles.

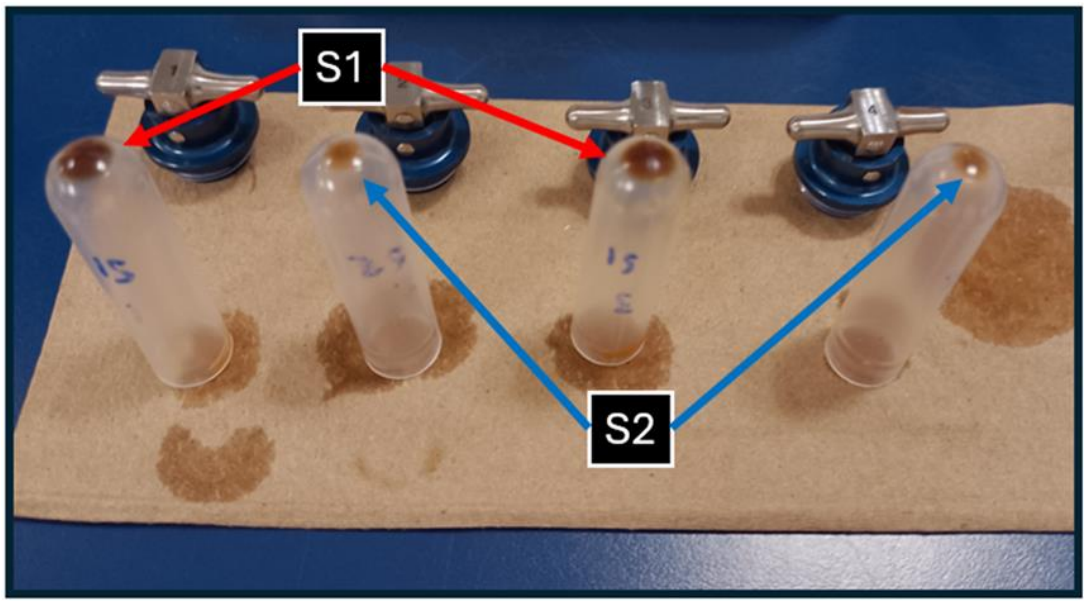

Figure 17. Supernatant concentration. (S1) Large dark brown pellet. (S2) Small clear brown pellets.

Following concentration, version 3 of the VLPs enrichment protocol introduced sucrose gradient separation for further refinement of particle isolation. Both supernatants produced visible bands; however, S1 presented a diffuse gradient zone with a bluish hue rather than a clearly defined band. The upper portion of S1's gradient zone displayed a distinct color, while the lower section appeared more diffuse. In contrast, S2 exhibited a thin, well-defined band with a pronounced white-blue color, indicating a more concentrated particle distribution. Neither gradient tube produced observable pellets in this phase (Figure 18).

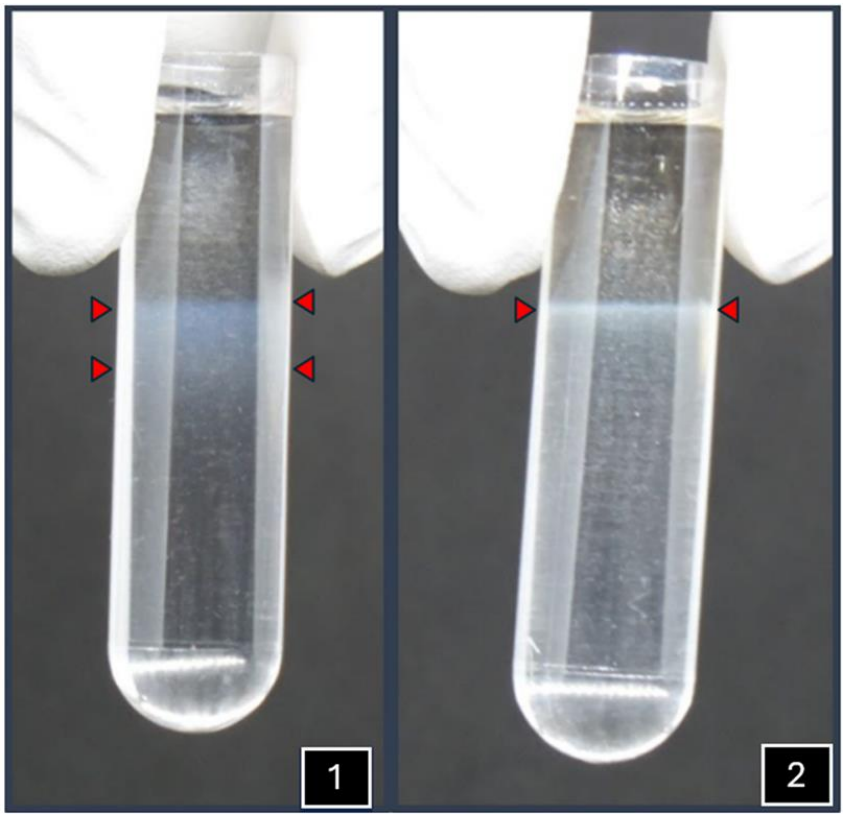

Figure 18**.** Enriched sample separation. (1) S1 gradient showing a visible gradient zone with a diffuse blue coloration. (2) S2 gradient displaying a well-defined and concentrated white-blue band.

Version 4 of the protocol incorporated an ultracentrifugation cleaning step for the bands fractioned from the gradient; the pellets obtained were small, transparent gel-like pellets visible only under careful inspection. Samples were labeled as "Band" from either S1 (solvent-free) or S2 (solvent-treated). While initial differences between S1 and S2 were observed, after enrichment and separation steps both displayed the same translucent, gel-like appearance after the cleaning step (Figure 19). This underscored the effectiveness of the cleaning phase in standardizing the samples for accurate categorization of viral particles.

Figure 19. Gradient band cleaning process. Gel-like, clear pellet formed after the cleaning process, marked with a red circle.

3.3 VLP identification and morphological classification

TEM imaging of samples from four versions of the protocol provided insights into the diversity and morphology of VLPs within both S1 and S2 supernatants. Across these versions, 237 VLPs were visualized, displaying a range of morphologies classified as either spherical/icosahedral (Group 1) or rod-like (Group 2).

In version 1 of the protocol, significant background material and cellular debris in TEM images complicated VLP identification, particularly in S2 samples, where complex backgrounds posed additional challenges (Figure 20).

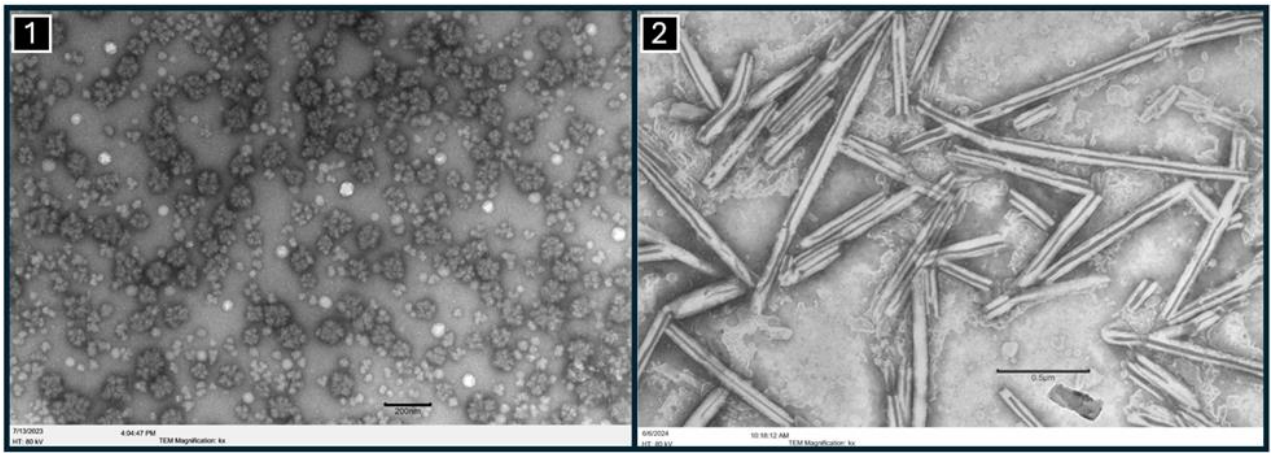

Figure 20. VLP enrichment protocols comparison. (1) First version of the enrichment protocol. Photo at 100 KX magnification showing substantial, unidentified material deposition, likely to consist of cellular debris or remnants, which limited VLP visibility. Origin of the sample, mixture of S1 and S2. (2) Last version of the enrichment protocol. Image at 100 KX magnification showing a marked reduction in unidentified material, significantly enhancing VLP visibility, Origin of the sample, S1.

However, the following protocol versions (2, 3 and 4), especially those incorporating sucrose gradient separation, progressively improved image clarity by reducing background material, facilitating easier identification of VLPs (Figures 21, 22, and 23). S1 samples maintained a uniform background, enabling relatively straightforward particle identification, while S2 backgrounds required additional refinement to achieve similar clarity.

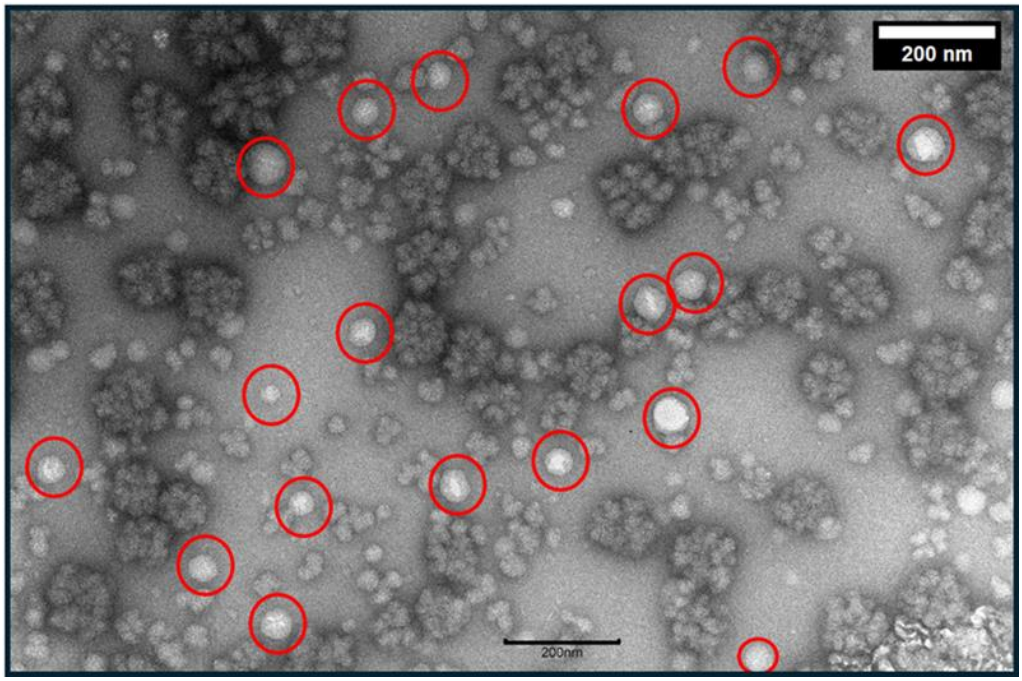

Figure 21. TEM images from VLP enrichment version 1 (mixture of S1 and S2). VLPs were observed (red circle) and large amounts of unidentified material in the background.

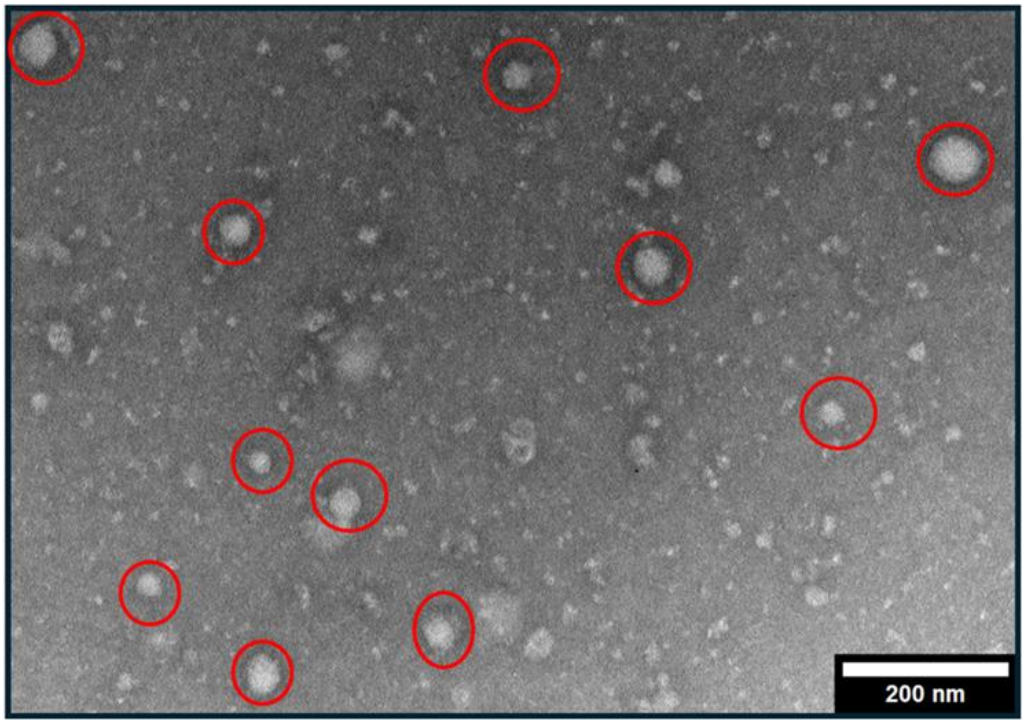

Figure 22. VLP enrichment version 2 (origin of sample S1). VLPs of spherical morphology (red circle). Noticeable reduction in the amount of material deposited on the grid improved the visualization of VLPs.

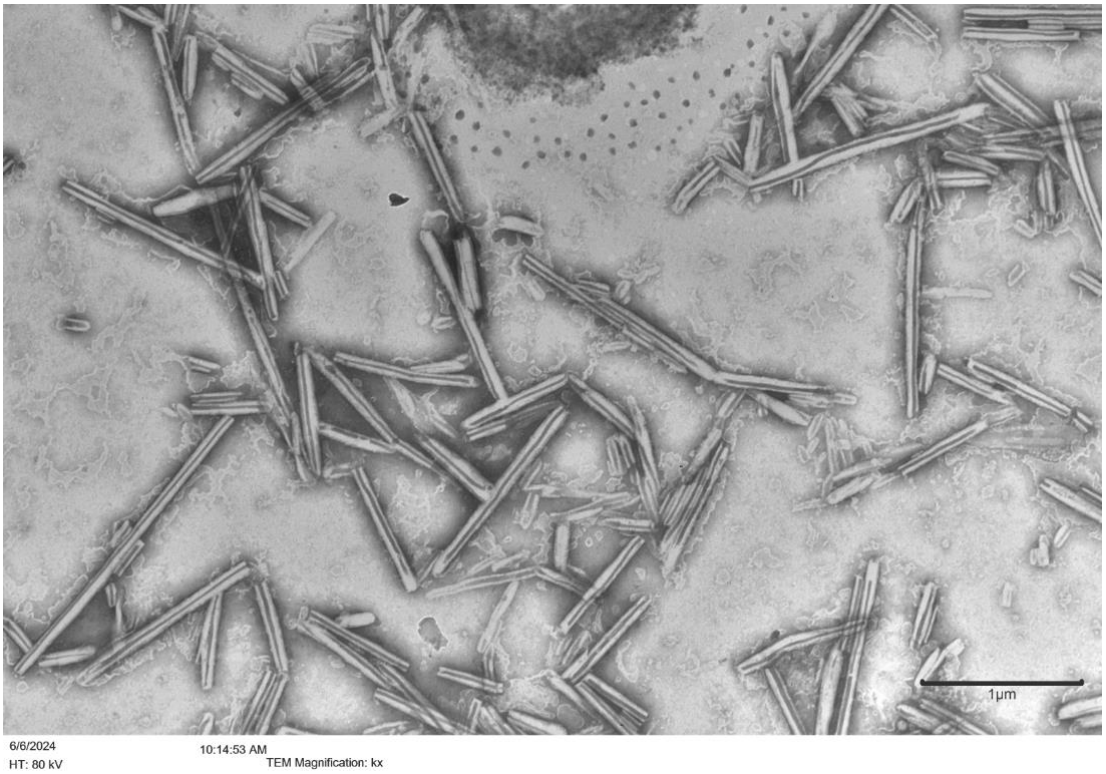

Figure 23. VLP enrichment version 4 (origin of sample S1). Rodlike VLP particles represent most of the observable objects, and the homogeneous background enhances the visualization of the VLPs.

Group 1 (spherical/icosahedral) VLPs, which ranged from 25 to 100 nm in diameter, predominantly clustered between 45–55 nm (Figure 24).

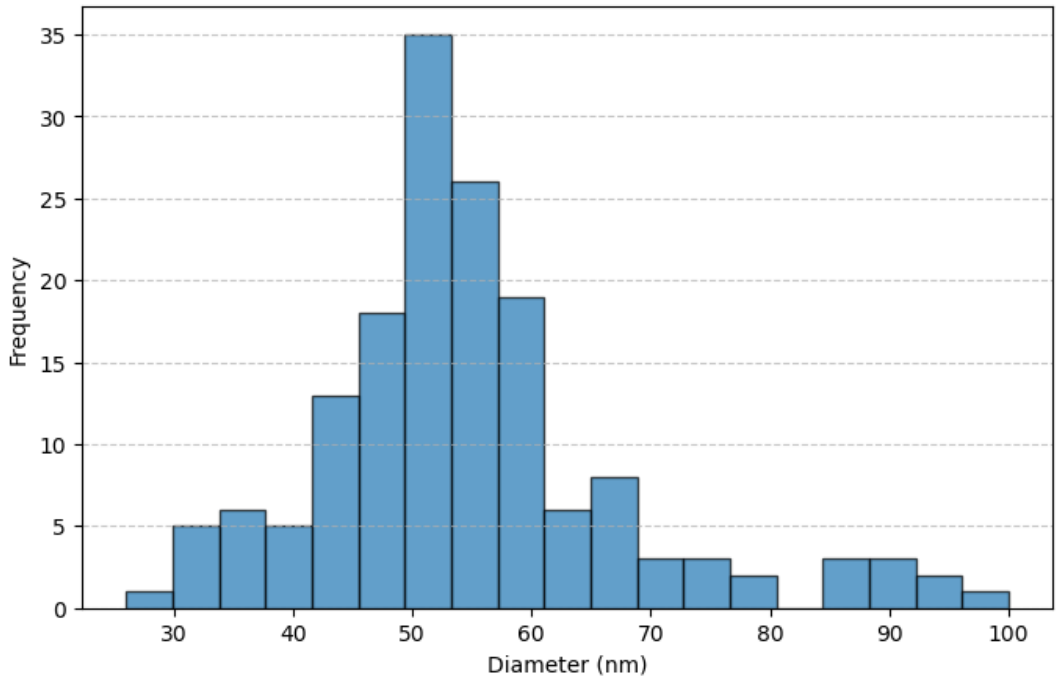

Figure 24. Spherical and icosahedral VLP population distribution.

Group 2 (rod-like) VLPs exhibited lengths between 154 nm and 2 µm, predominant cluster within 550-750 nm with consistent morphology observed across most TEM examinations (Figure 25).

Figure 25. Rodlike VLP population distribution

3.4 Comparative morphology with known viral families

Some of the observed VLPs from group 1 matched virions from several known viruses in terms of size and morphology, including iflavirus (26–30 nm), dicistrovirus (30 nm), and reovirus (60–90 nm), aligning with viral sequences previously reported by our research group (Duarte de Jesús, 2020) (Figure 26).

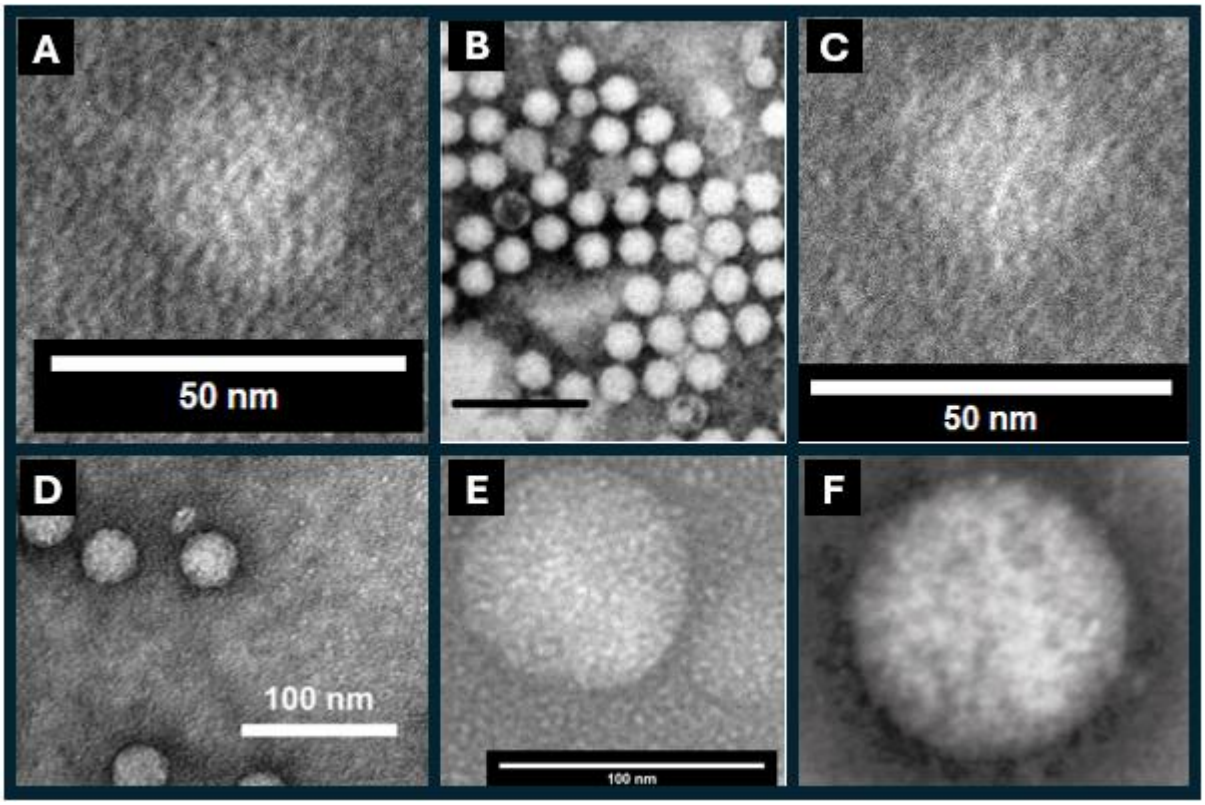

Figure 26. The observed VLPs show morphological similarities with known viral particles. (A) A 27 nm VLP within the size range of iflavirus particles, compared to (B), a 27–30 nm isometric particles from flacherie virus (ICTV, reference bar, 100 nm). (C) A 30 nm VLP within the size range of dicistrovirus particles, compared to (D), a 30 nm particle from triatoma virus (ICTV). (E) A 90 nm VLP within the size range of reovirus particles, compared to (F), virion of Dacus oleae idenoreovirus 4 (DolRV4) stained with sodium phosphotungstate, approximately 70 nm (ICTV).

3.5 Morphotype identification in rod-like VLPs

Two distinct morphotypes of rod-like VLPs were identified in both S1 and S2 samples. Morphotype 1, observed predominantly in S2, had an irregular surface with an average diameter around 100 nm and occasionally displayed underlying structures suggestive of a coating (either lipid or protein-based) that may have been compromised during the enrichment protocol. Morphotype 2, observed in both S1 and S2, had a more uniform rod-like shape, with a consistent diameter of approximately 80 nm. It is possible that these two morphotypes represent the same particle type, with Morphotype 1 retaining a coating structure and Morphotype 2 lacking it (Figure 27).

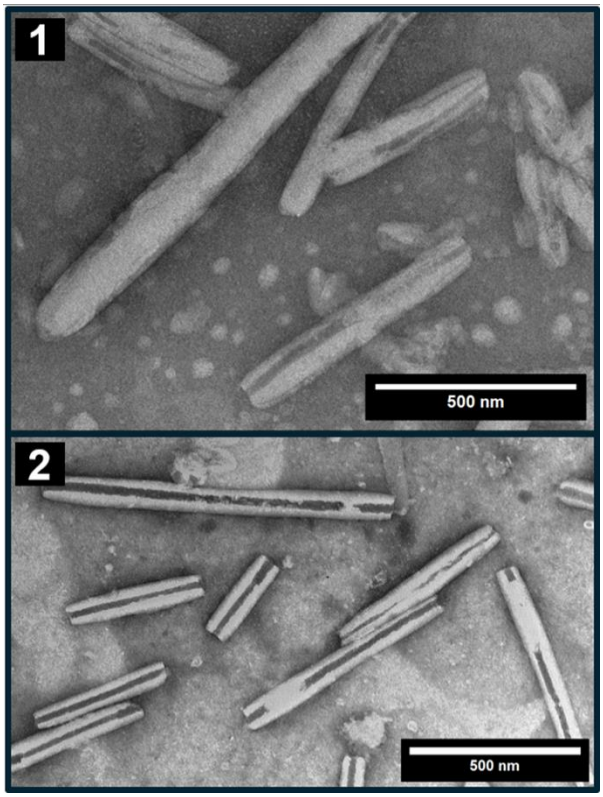

Figure 27. Rodlike VLP morphotypes. (1) Morphotype 1, 100 nm diameter on average. (2) Morphotype 2, 80 nm diameter on average.

In addition to the histogram distributions (Figures 23 and 24), the TEM images confirmed that spherical (Group 1) and rod-like (Group 2) particles were consistently present across samples. While rod-like particles were more prominent in S2, both categories provided a representative picture of VLP diversity in the samples.

In the TEM images, VLPs from S1 origin exhibited spherical particles ranging between approximately 26 nm and 56 nm in diameter and VLPs with rod-like morphologies, with both Morphotype 1 and Morphotype 2 present. Morphotype 2 appeared more frequently in these samples (Figure 28).

In contrast, VLPs from S2 origins, during version 4 of the protocol, displayed only rod-like particles. Compared to the S1 samples, the presence of these VLPs was more prominent. Both morphotypes were observed, with a higher occurrence of Morphotype 1 in S2 samples compared to those from S1 origin (Figure 29).

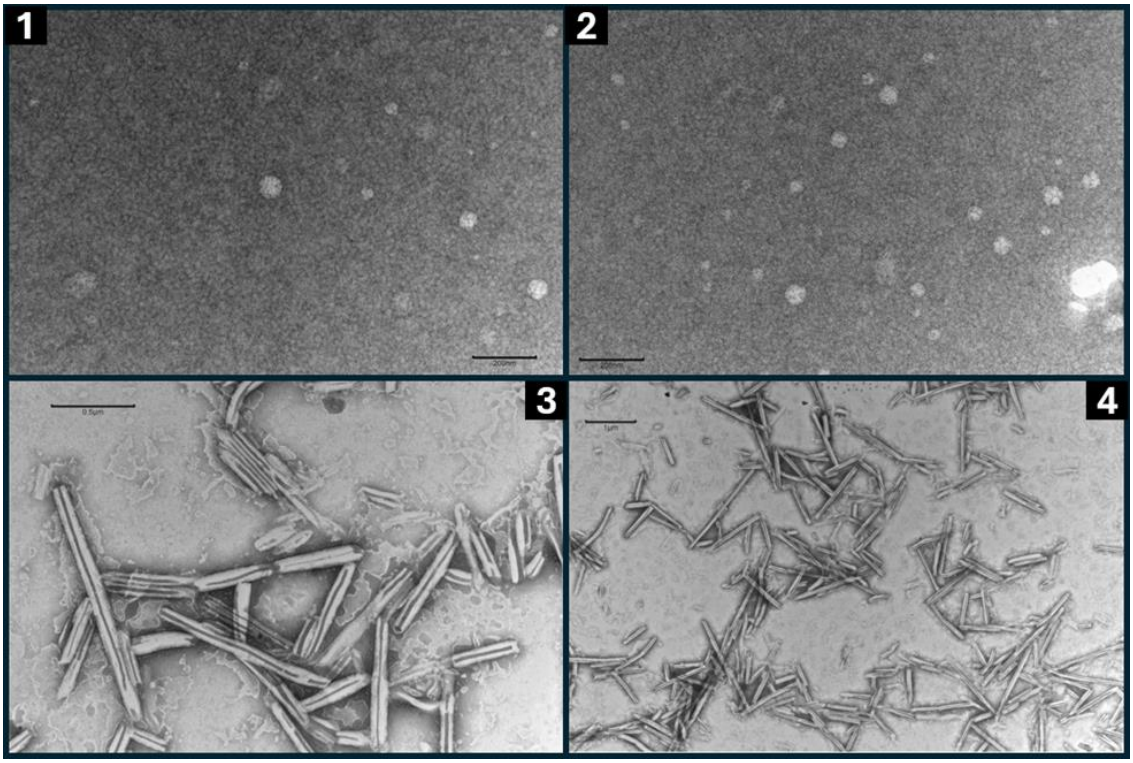

Figure 28. TEM images from S1 origin. (1, 2) Spherical particles with an irregular surface. Reference bar, 200 nm. (3, 4) Rodlike VLPs from morphotype 2. Reference bar, 0.5 µm (3) or 1 µm (4).

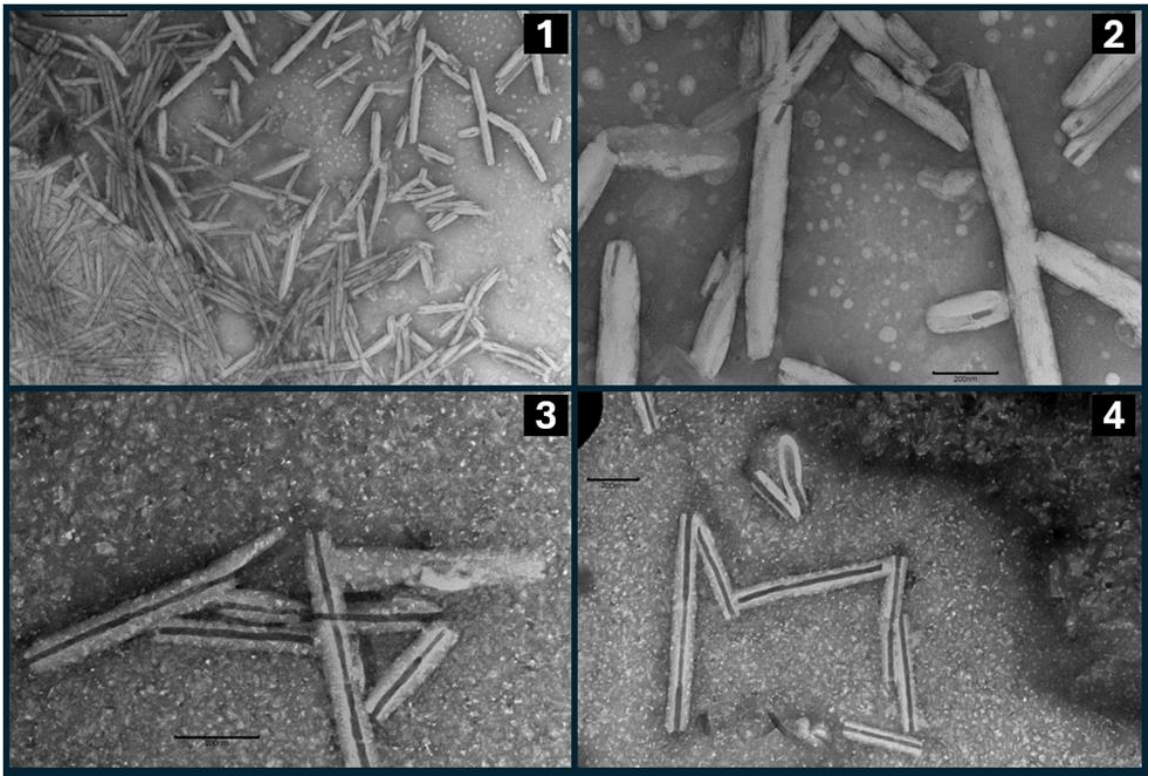

Figure 29. TEM images from S2 origin. (1) Large quantities of rodlike VLPs Morphotype 1. Reference bar, 1 µm. (2) Close up to rodlike VLPs Morphotype 1. Reference bar, 200 nm. (3, 4) Rodlike VLPs of Morphotype 2. Reference bar, 200 nm.

3.6 Infectivity assay and ATM efficiency

3.6.1 Temperature influence on eclosion timing

Mealybugs from the breeding stock colony were used in the eclosion experiment and exhibited oviposition typically within 1–2 days, with most activity occurring between days 2 and 3 across all experimental sets. Eclosion generally began 4–5 days after oviposition, with crawler emergence noted around days 7–8. Peak eclosion occurred between 7–9 days post-oviposition, corresponding to days 10–15 of the experiment. After this peak, eclosion rates declined noticeably around 10–12 days post-oviposition, with a significant decrease in crawler numbers observed between days 13 and 18. Temperature appeared to influence crawler emergence, as suggested by observational trends. Higher temperatures, particularly those above 26°C, had an observable effect on the rate of crawler emergence. An observable increase in crawler numbers was registered when temperatures reached 28°C, a trend consistent across multiple sets. The effect of temperature was not immediate, as increases in crawler emergence were observed approximately three days after temperature rises. Specifically, a temperature rise on days 11–12 corresponded with increased crawler births on day 15, and a temperature rise on day 14 was followed by a crawler increase on day 17. The graph in Figure 30 illustrates the cumulative emergence of new crawlers across all four sets (totaling 20 ATMs) and highlights the overall influence of temperature on eclosion rates over the experiment duration.

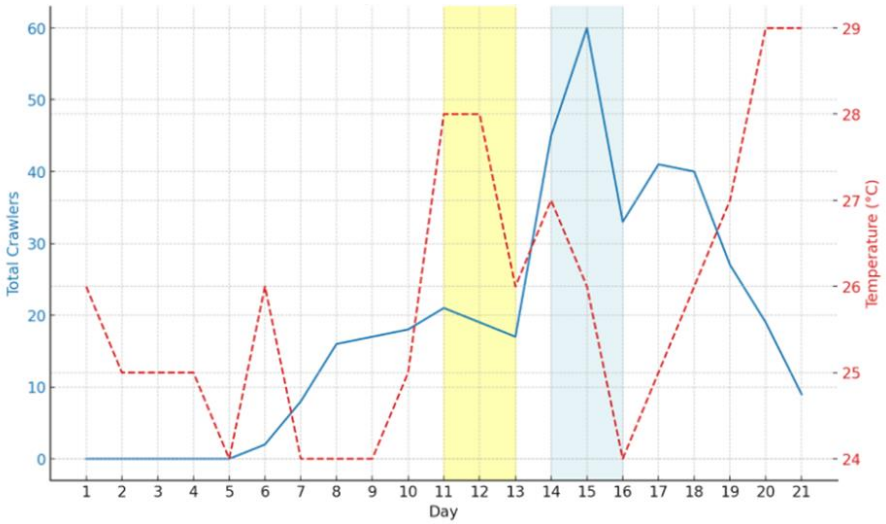

Figure 30. Temperature effect on eclosion. Cumulative number of emerging crawlers (blue line). Temperature (red line). Days 11-13: Temperature rose to 28°C (yellow zone), leading to an increase in crawler emergence days 14-16 (blue zone).

The data gathered on eclosion timing, peak periods, and the impact of temperature informed the optimal timeline and conditions for the infectivity assay, allowing for greater accuracy and consistency in future studies.

3.6.2 ATM treatment acquisition efficiency

VLP suspension acquisition was confirmed by examining crawlers for visible dye, distinguishing those that had ingested the dyed suspension (Figure 31). A total of 42.32% of crawlers showed evidence of feeding on the dyed suspension (Table 1). This percentage reflects the ATM's effectiveness in delivering the suspension to the crawlers. The ATM structure was sturdy and easy to handle, allowing for straightforward observation of oviposition and crawler behavior.

Figure 31. Dyed suspensions acquisition. (1) Two 1st instar crawlers, dorsal view; left not dyed, right dyed. (2) Same crawlers, ventral view.

Table 1. ATM percentage of acquisition using dyed substrate during a 5-day acquisition window from peak eclosion onset, showing total dyed, and percentage of dyed crawlers per trial.

ATM	Total Crawlers	Dyed Crawlers	Percentage (%)
1	46	23	50
2	30	9	30
3	37	16	43.24
4	27	5	18.52
5	26	9	34.62
6	70	32	45.71
7	40	27	67.5
8	97	43	44.33
9	66	32	48.48
10	76	31	40.79
Average			**42.32**

3.6.3 Preliminary infectivity assay

Treatment A (TA) consisted of a stock VLP suspension. Treatment B was a diluted VLP suspension (1:10), and treatment C (TC), a solution without VLP suspension. Acquisition of the treatments was confirmed by the visualization of stained guts in the treated crawlers, indicating successful uptake. Maximal acquisition was observed in TA (Table 2).

Table 2. Acquisition rate for infectivity assay

Treatment	Total crawlers	Total treated crawlers	Average treatment acquisition	Treated crawlers for each PI
TA	253	135	53.36%	45
TB	244	90	36.89%	30
TC	256	72	28.13%	24

Crawlers from each treatment were evenly divided into three reservoirs corresponding to post-inoculation periods (PI) of varying durations: PI1 (4 days), PI2 (10 days), and PI3 (128 days). Crawlers that survived the PI were registered after excluding deaths by mechanical sources derived by reservoir manipulation (Tables 3, 4).

Table 3. Survival rates of crawlers for PI1

Treatment	Treated crawlers	Death crawlers	Survival percentage
TA	45	5	88.88%
TB	30	7	76.66%
TC	24	0	100%

Table 4. Survival rates of crawlers for PI2

Treatment	Treated crawlers	Death crawlers	Survival percentage
TA	45	12	73.33%
TB	30	10	33.33%
TC	24	13	45.83%

For PI3 the collected biomass was divided into two categories based on source location and composition. Type 1 biomass, representing material gathered from the reservoir lid area, was relatively low across treatments. Type 2 biomass, encompassing all material within the reservoir and including mealybugs at various developmental stages along with cotton-like structures, was notably higher. TA produced the largest volume of biomass along with the greatest quantity of cotton-like structures, followed by TB, while TC exhibited the lowest number of cotton-like structures and overall biomass (Table 5).

Table 5. Biomass collected after PI3

Treatment	Treated crawlers	Type 1 biomass (g)	Type 2 biomass (g)
TA	45	1.114	3.433
TB	30	0.016	0.514
TC	24	0.001	0.213

Over the 133 days of the experiment, two observed instances of adult male emergence across all treatments, and at the experiment conclusion, presence of pupas were noticed. The presence of adult males at the time of biomass collection, alongside newborn crawlers, suggested the initiation of a third generation.

Chapter 4. Discussion

4.1 Differences between S1 and S2 in the dual particle extraction approach

The term virus-like particle (VLP) was employed in this study to describe the particles observed through TEM, as their structure and morphology closely resembled virions. Although their genetic content has not yet been analyzed, the consistent presence of these particles across different micrographies and their abundance strongly suggested that they were not artifacts. The defined and repetitive structures reduced the likelihood of these observations being the result of imaging aberrations.

This use of the term VLP reflected our cautious approach, pending further molecular and infectivity analyses to confirm their viral nature. For instance, in the case of the rod-like particles observed, the term "virion" or "virus" could only be applied if subsequent analyses confirmed that these particles contained genetic material and demonstrated infectivity. Until such confirmation is achieved, referring to them as VLPs ensures accuracy and avoids premature assumptions about their biological function or viral identity.

The dual enrichment approach aimed to assess whether the methodology effectively generated distinct differences between samples, S1 and S2. A notable difference was observed during the double extraction process, which initially involved extraction without solvent, followed by a chloroform:n-butanol (1:1 v/v) treatment of the pellet. This procedure maximized the use of limited sample material and aligned with the approaches of Luria et al. (2020), who also used a chloroform and n-butanol mixture for selective VLP enrichment, and Feng et al. (2017), who employed chloroform alone for initial extraction but primarily relied on density gradients for particle separation. Duarte de Jesús' (2020) modified version of Feng's protocol included dual chloroform-based extractions to enhance lipid dissolution and particle release.

Chloroform, a non-polar solvent, effectively disrupted lipid membranes and denatured proteins, facilitating the separation of VLPs from cellular debris. However, the addition of n-butanol, a moderately polar solvent, enhanced the overall extraction process by promoting the gradual dissolution of lipids while maintaining the structural integrity of the VLPs (Wijesundara et al., 2022). This combination allowed for a balance between thorough lipid removal and preservation of protein stability. The integration of n-butanol mitigated the potentially harsh effects of chloroform, reducing the risk of compromising VLP integrity during extraction.

Apparent differences were observed between S1 and S2 following the extraction and separation processes. The S1 gradient displayed a larger, diffuse band with a distinct blue hue, suggesting the presence of a heterogeneous sample with variability in VLP morphology and density. In contrast, the S2 gradient yielded a sharp, well-defined band with blue and white hues, indicative of a more uniform particle composition. The more concise and defined band observed in S2 compared to S1 may have reflected a wider range of VLP sizes in S1 in comparison to S2.

While this interpretation provided valuable insights, further experimentation would be required to confirm it. To date, no other studies on vine mealybugs have employed a separation technique such as the one used in this work, specifically sucrose gradient ultracentrifugation, to study the diversity of VLPs present within the vine mealybug. The closest comparable methodology was that of Luria et al. (2020), though their approach did not include a separation step, leaving no direct basis of reference. Additional comparison could be drawn with the work of Duarte de Jesús (2020), who used a different solvent proportion (5 mL of chloroform for every 10 mL of PBS buffer), whereas this study utilized a 1:1 mixture of chloroform and n-butanol in a proportion of 600 µL of buffer to 60 µL of the solvent mixture. Duarte de Jesús reported observing filamentous VLP resembling closterovirus virions and spherical particles potentially aggregating into larger structures. The study also noted a limited number of VLPs recovered, highlighting challenges in particle enrichment.

To further investigate and validate the differences observed in the S1 and S2 bands formed after gradient separation, future experiments should assess the current enrichment methodology by comparing it with bands formed from samples treated with varying solvent volumes. Additionally, visualizing the VLPs resulting from these variations using TEM will enhance our understanding of how these variables influence VLP obtained during gradient after the solvent treatments procedures.

4.2 VLPs morphology in TEM visualizations

Direct evidence linking viral particles to vine mealybugs remains limited. However, studies have identified dicistroviruses in related mealybug species, providing relevant context. Luria et al. (2020) reported a novel cripavirus in the cotton mealybug (*Phenacoccus solenopsis*). Similarly, Martinez-Mercado et al. (2022) identified a dicistrovirus in vine mealybugs, designated Planococcus ficus-associated dicistrovirus 1 (PfDV1). Their analysis showed high sequence similarity (89–92%) to the virus identified by Luria et al. (2020), suggesting both are isolates of the same species. In our study, we observed and measured 30 nm virus-like particles consistent with the morphology and size range of dicistrovirus virions. These findings

highlight the potential role of dicistroviruses in vine mealybug populations, though further research is needed to fully understand their impact.

In Duarte de Jesús study, TEM analysis revealed spherical VLPs with a granular surface measuring approximately 150 nm, along with hexagonal, inclusion-like structures that suggested the presence of viral aggregates or occlusion bodies. However, although viral sequences belonging to the family *Rhabdoviridae* and the order *Bunyavirales* (enveloped RNA viruses with bullet-shaped and pleomorphic particle morphologies, respectively) were reported, in this study the only spherical VLPs were measured within the range of 80-100 nm would match the corresponding particle of virions from the *Bunyavirales* order while VLPs of bullet shape were not clearly visualized in this study. This discrepancy highlighted an opportunity for future targeted approaches to enhance the visualization and characterization of these specific viral morphologies.

In this study, two main VLP categories were identified: spherical/icosahedral and rod-like particles. Most spherical VLPs clustered around 50–55 nm diameter (Figure 24). These particles were consistently observed across multiple protocol iterations, with improved clarity achieved through methodological enhancements in extraction and separation techniques. The 50–55 nm particles aligned with the documented dimensions of reovirus core particles (50–60 nm), which are subviral structures involved in the viral replication cycle (ICTV, 2011). Their presence may be attributed to the loss of the outer layer during enrichment protocols or to the virus being at different maturation stages at the time of sample processing. Further characterization is necessary to determine their nature.

Rod-like particles were detected following sucrose gradient ultracentrifugation in protocol versions 3 and 4, coinciding with the inclusion of mealybugs from sites marked in blue on the recollection map (Figure 3). These rod-like VLPs measured between 154 nm and 2 µm length, with a predominant cluster between 550–750 nm (Figure 25). Their size distribution was analyzed using histogram, providing visual aid to identify clustering patterns while accounting for the broad size range of these particles. The use of sucrose gradient ultracentrifugation effectively facilitated the separation and visualization of these particles.

To the best of our knowledge, this study represents the first report of rod-like VLPs in vine mealybugs. Unlike previous studies (Luria et al., 2020; Duarte de Jesús, 2020), which did not mention such particles, our observations further supported by reverse-image searches revealed rod-like VLPs that can be categorized into two distinct morphotypes. Morphotype 1 features an outer enveloping layer with an average diameter of 100 nm, whereas morphotype 2, with an average diameter of 80 nm, lacks this layer

and displays a continuous canal-like structure averaging 19 nm. These structural distinctions suggest unique features not previously documented in vine mealybug VLP studies. Future studies to further characterize morphotype 1 could build upon these findings by incorporating advanced techniques, such as lipid staining assays with dyes like Nile Red or LipidTOX (Criglar et al., 2022; Raghunath et al., 2022), detergent sensitivity assays using Triton X-100 or sodium deoxycholate analyzed via electrophoresis, and lipid analysis through thin-layer chromatography (van Til et al., 2008) or high-performance liquid chromatography. These methods could provide additional confirmation of the presence of lipid envelopes and further enhance the understanding of VLP characteristics without relying solely on microscopy.

Notably, the appearance of these rod-like VLPs was first detected when mealybugs from one specific collection site (site 6) were incorporated into the enrichment protocol. Mealybugs from site 6 exhibited pronounced fragility during mechanical processing reminiscent of the cuticle rupture and internal liquefaction observed in baculovirus-infected Lepidoptera larvae (Harrison & Hoover, 2012) and displayed a distinct deep brown coloration upon maceration, in contrast to the amber-orange hue of samples from other sites. These observations, together with Duarte de Jesús' (2020) findings of homologous genes related to baculoviruses, nudiviruses, and polydnaviruses, raise the possibility that the rod-like VLPs share morphological similarities with baculovirus virions (albeit with differences in length and lacking occlusion bodies). TEM images revealed a prominent presence of rod-like VLPs only after including mealybug samples from all collection sites. This observation suggests the possibility of ongoing replication if these VLPs originate from a single site. Currently, based on observations of mealybugs from site 6, we suspect this location could be the source of these VLPs. However, this hypothesis remains unconfirmed, and further investigations such as targeted enrichment protocols only with samples from this site are necessary to determine the exact origin of the VLPs.

Future investigations should elucidate the factors driving the variation in observed rod-like VLP lengths while their diameter and morphology remain consistent. Possible explanations include different maturation stages, as observed in viral particle maturation (Garoff et al., 1998), or aggregation phenomena influencing particle organization (Pradhan et al., 2022), though these remain speculative.

To test these hypotheses, sequencing analyses could identify these VLPs, while infectivity assays followed by TEM observations at different post-inoculation periods to evaluate their infectivity capabilities if they possess and monitor structural changes over time. This approach could determine whether these particles undergo developmental transitions or result from aggregation dynamics.

4.3 Preliminary infectivity assay for vine mealybugs

Maintaining temperatures between 25–29°C resulted in a higher number of crawlers emerging from ATMs, aligning with previous findings that associate these conditions with increased mealybug reproductive rates (Mohamed, 2017; Daane et al., 2012). Given this temperature effect and the established eclosion timeline, treatments were administered during the peak eclosion period (days 10–15). This timing maximizes crawler exposure to VLP suspensions while minimizing potential degradation due to environmental stress, helping preserve VLP stability.

To enhance VLP acquisition in early-stage crawlers, modifications were made to the ATM design proposed by Arora et al. (2020). Adjustments included sanding the inner surface and incorporating a wrinkled membrane to improve feeding efficiency. These adaptations allowed around 42.32% of crawlers to ingest the dyed substrate. Unlike Arora et al. study, which focused on RNA interference (RNAi) in older instars of grape mealybug (*Pseudococcus maritimus*), this study emphasized early-stage crawlers to assess the potential cumulative effects of VLP exposure across developmental stages.

The acquisition rates of treatments showed a clear preference pattern, with TA > TB > TC. This trend may be attributed to the presence of residual sucrose in the VLP suspension (TA), a lower sucrose concentration in the diluted treatment (TB), and its absence in the control (TC). Sucrose has been shown to influence feeding behavior in the cotton mealybug, a close relative of the vine mealybug (Mohamed Adam et al., 2019), which may explain the increased uptake observed in TA and, to a lesser extent, in TB.

Survival rates varied among treatments post-inoculation, with differences becoming more pronounced over time. In PI1 (4 days), TC showed 100% survival, while TA and TB had slightly lower rates (88.88% and 76.66%, respectively). By PI2 (10 days), TA maintained higher survival (73.33%), whereas TB and TC declined to 33.33% and 45.83%, respectively. These trends suggest that treatment composition may have influenced survival, with TA's higher residual sucrose potentially mitigating nutritional stress over a prolonged period. In contrast, the lower sucrose content in TB and its absence in TC may have contributed to nutritional limitations becoming more apparent over time, leading to increased mortality.

However, further experiments using additional dilution levels are needed to better understand the extent to which sucrose concentration impacts vine mealybug survival and to refine the treatment conditions for future studies.

The biomass collected at the end of PI3 further supported these observations. TA yielded the highest Type 2 biomass, which included mealybugs at various developmental stages and abundant cotton-like structures. TB produced a lower but still significant biomass, whereas TC resulted in the least amount of material collected. The disparity in biomass accumulation could be attributed to differences in initial mealybug numbers, mortality rates, and feeding behavior influenced by treatment composition.

Additionally, the presence of adult males and pupae at the time of biomass collection, along with the emergence of newborn crawlers, indicated the onset of a third generation across all treatments. This suggests that, despite differences in mortality rates, generational cycling occurred throughout the experiment.

Chapter 5. Conclusions

This study achieved significant methodological advancements in VLP isolation and visualization from vine mealybugs. A total of 259 distinct VLPs were successfully documented, with precise morphological measurements and reference images captured for further analysis.

A refined enrichment protocol was developed, enabling the visualization of two VLP categories: spherical/icosahedral and rod-like particles, each with distinct size and structural features. While some spherical VLPs exhibited morphologies consistent with virions of iflavirus, dicistrovirus and reovirus, the rod-like VLPs lacked clear taxonomic classification, suggesting they may represent a novel, uncharacterized viral entity. Their consistent presence across visualized micrographics highlights their potential significance, warranting further investigation.

Future research should focus on confirming the identity of these rod-like VLPs through genomic sequencing and comparative structural analysis. Additionally, long-term infectivity assays could assess their biological relevance, particularly their impact on mealybug population dynamics and reproductive success.

Finally, the infectivity assay provided preliminary insights into VLP-host interactions, complementing improvements in VLP enrichment methodologies. These findings establish a foundation for future virome research, particularly in evaluating VLPs for potential applications in VLPs-based pest control strategies.

Bibliography

Arora, A. K., Clark, N., Wentworth, K. S., Hesler, S., Fuchs, M., Loeb, G., & Douglas, A. E. (2020). Evaluation of rna interference for control of the grape mealybug pseudococcus maritimus (Hemiptera: Pseudococcidae). *Insects, 11*(11), 1–15. https://doi.org/10.3390/insects11110739

Atallah, S. S., Gómez, M. I., Fuchs, M. F., & Martinson, T. E. (2012). Economic impact of grapevine leafroll disease on Vitis vinifera cv. Cabernet franc in Finger Lakes vineyards of New York. *American Journal of Enology and Viticulture, 63*(1), 73–79. https://doi.org/10.5344/ajev.2011.11055

Bonning, B. C. (2020). The insect virome: Opportunities and challenges. Current Issues in Molecular *Biology, 34*, 1–12. https://doi.org/10.21775/9781912530083.01

Bonning, B. C., & Miller, W. A. (2010). Dicistroviruses. In Annual Review of Entomology (Vol. 55, pp. 129–150). https://doi.org/10.1146/annurev-ento-112408-085457

Cerezo Limón, F. J. B. (2022). *Caracterización inicial del genoma del virus del piojo harinoso de la vid Planococcus ficus-associated reovirus 1 mediante técnicas moleculares* [Tesis de licenciatura, Universidad de Guadalajara]. Tesis sin publicar

Criglar, J. M., Estes, M. K., & Crawford, S. E. (2022). Rotavirus-Induced Lipid Droplet Biogenesis Is Critical for Virus Replication. In *Frontiers in Materials (Vol. 13)*. Frontiers Media S.A. https://doi.org/10.3389/fphys.2022.836870

Cocco, A., Pacheco da Silva, V. C., Benelli, G., Botton, M., Lucchi, A., & Lentini, A. (2021). Sustainable management of the vine mealybug in organic vineyards. *Journal of Pest Science, 94*(1), 153–185. https://doi.org/10.1007/s10340-020-01305-8

Daane, K. M., Yokota, G. Y., Walton, V. M., Hogg, B. N., Cooper, M. L., Bentley, W. J., & Millar, J. G. (2020). Development of a mating disruption program for a mealybug, Planococcus ficus, in vineyards. *Insects, 11*(9), 635. https://doi.org/10.3390/insects11090635

Delgado Silva, T. I. (2022). *Caracterización inicial de virus del género Marafivirus en Baja California, México* [Tesis de licenciatura, Universidad Veracruzana. Tesis sin publicar

Duarte de Jesús, J. L. (2020). *Identificación de secuencias genómicas virales en el piojo harinoso de la vid (Planococcus ficus Signoret, 1875) presente en viñedos de Ensenada, Baja California* [Tesis de maestría, Centro de Investigación Científica y de Educación Superior de Ensenada (CICESE)]. Repositorio institucional https://biblioteca.cicese.mx/catalogo/tesis/ficha.php?id=25817

Feng, Y., Krueger, E. N., Liu, S., Dorman, K., Bonning, B. C., & Miller, W. A. (2017). Discovery of known and novel viral genomes in soybean aphid by deep sequencing. *Phytobiomes, 1*(1), 36–45. https://doi.org/10.1094/PBIOMES-11-16-0013-R

Fu Castillo, & Grageda Grageda. (2002). Fu-Castillo-2002-Biocontrol-of-Planococcus-ficus. Instituto Nacional de Investigaciones Forestales, Agrícolas y Pecuarias. https://www.cabi.org/wp-content/uploads/Fu-Castillo-2002-Biocontrol-of-Planococcus-ficus.pdf

Garoff, H., Hewson, R., & Opstelten, D. J. (1998). Virus maturation by budding. Microbiology and *Molecular Biology Reviews, 62*(4), 1171–1190. https://doi.org/10.1128/MMBR.62.4.1171-1190.1998

Gobierno de México. (2022). Ficha técnica: Piojo harinoso de la vid (Planococcus ficus). Gobierno de México. Recuperada el 6 de Junio 2023, de https://www.gob.mx/cms/uploads/attachment/file/778937/Ficha_t_cnica_Piojo_harinoso_de_la_vid_Planococcus_ficus_2022.pdf

González Andrade, S. (2015). Cadena de valor económico del vino de Baja California, México. *Estud. Front., 16*(32), 163–193. http://www.scielo.org.mx/scielo.php?script=sci_arttext&pid=S0187-69612015000200006&lng=es&nrm=iso

Hammond GW, Hazelton PR, Chuang I, Klisko B. Improved detection of viruses by electron microscopy after direct ultracentrifuge preparation of specimens. J Clin Microbiol. 1981 Aug;14(2):210-21. doi: https://doi.org/10.1128/jcm.14.2.210-221.1981

Handley, S. A. (2016). The virome: A missing component of biological interaction networks in health and disease. *Genome Medicine, 8*(32). https://doi.org/10.1186/s13073-016-0287-y

Harrison, R. L., & Hoover, K. (2012). Baculoviruses and other occluded insect viruses. Insect *Pathology, 4*, 73–110. https://doi.org/10.1016/B978-0-12-384984-7.00004-X

International Committee on Taxonomy of Viruses (ICTV). (2011). Reoviridae. In Virus taxonomy: Ninth report of the International Committee on Taxonomy of Viruses. Retrieved 7th of July 2024 from https://ictv.global/report_9th/dsRNA/Reoviridae

Katz, D., & Kohn, A. (1984). Immunosorbent electron microscopy for detection of viruses. Adv. Virus Res., 29, 169–194. DOI: https://doi.org/10.1016/S0065-3527(08)60408-X

Liu, C. L. C., Kuchma, O., & Krutovsky, K. V. (2018). Mixed-species versus monocultures in plantation forestry: Development, benefits, ecosystem services and perspectives for the future. *Global Ecology and Conservation, 15*, e00419. https://doi.org/https://doi.org/10.1016/j.gecco.2018.e00419

Luria, N., Smith, E., Lachman, O., Laskar, O., Sela, N., & Dombrovsky, A. (2020). Isolation and characterization of a novel cripavirus, the first Dicistroviridae family member infecting the cotton mealybug Phenacoccus solenopsis. *Archives of Virology, 165*. https://doi.org/10.1007/s00705-020-04702-7

Mateu, M. G. (2012). Mechanical properties of viruses analyzed by atomic force microscopy: A virological perspective. *In Virus Research (Vol. 168*, Issues 1–2, pp. 1–22). https://doi.org/10.1016/j.virusres.2012.06.008

Meulenberg, J. J., & Petersen-den Besten, A. (1996). Identification and characterization of a sixth structural protein of Lelystad virus: the glycoprotein GP2 encoded by ORF2 is incorporated in virus particles. *Virology, 225*(1), 44–51 doi: https://doi.org/10.1006/viro.1996.0573

Miyamoto, H., Okamoto, H., Sato, K., Tanaka, T., & Mishiro, S. (1992). Extraordinarily low density of hepatitis C virus estimated by sucrose density gradient centrifugation and the polymerase chain reaction. In *Journal of General Virology (Vol. 73)* doi: 10.1099/0022-1317-73-3-715

Mohamed Adam, A. H., Mohamed, N. A., & Taha, A. K. (2019). Laboratory Studies on the Host Preference of Cotton Mealybug 'Phenacoccussolenopsis' Tinsely (Hemiptera: Pseudococcidae) in Khartoum State, Sudan. *Journal of Agronomy Research, 1*(3), 35–43. https://doi.org/10.14302/issn.2639-3166.jar-18-2576

Nasukawa, T., Uchiyama, J., Taharaguchi Satoshi and Ota, S., Ujihara, T., Matsuzaki, S., Murakami, H., Mizukami, K., & Sakaguchi, M. (2017). Virus purification by CsCl density gradient using general centrifugation. Arch. *Virol., 162*(11), DOI: 10.1007/s00705-017-3513-z

Pradhan, S., Varsani, A., Leff, C., Swanson, C. J., & Hariadi, R. F. (2022). Viral aggregation: The knowns and unknowns. *Viruses, 14*(2), 438. https://doi.org/10.3390/v14020438

Qin, P., Du, E.-Z., Luo, W.-T., Yang, Y.-L., Zhang, Y.-Q., Wang, B., & Huang, Y.-W. (2019). Characteristics of the life cycle of porcine Deltacoronavirus (PDCoV) in vitro: Replication kinetics, cellular ultrastructure and virion morphology, and evidence of inducing autophagy. *Viruses, 11*(5), 455. https://doi.org/10.3390/v11050455

Raghunath, G., Chen, Y. C., Marin, M., Wu, H., & Melikyan, G. B. (2022). SERINC5-Mediated Restriction of HIV-1 Infectivity Correlates with Resistance to Cholesterol Extraction but Not with Lipid Order of Viral Membrane. *Viruses, 14*(8). https://doi.org/10.3390/v14081636

Richert-Pöggeler, K. R., Franzke, K., Hipp, K., & Kleespies, R. G. (2018). Electron microscopy methods for virus diagnosis and high resolution analysis of viruses. Front. *Microbiol., 9*, 3255. https://doi.org/10.3389/fmicb.2018.03255

Roingeard, P. (2008). Viral detection by electron microscopy: past, present and future. *Biol. Cell, 100*(8), 491–501. doi: https://doi.org/10.1042/BC20070173

Secretaría de Agricultura y Desarrollo Rural. (2022, July 29). Generaron productores de vid de Baja California derrama económica superior a los $595 MDP. Gobierno de México. https://www.gob.mx/agricultura%7Cbajacalifornia/articulos/generaron-productores-de-vid-de-baja-california-derrama-economica-superior-a-los-595-mdp

Solaiman, R. H. A., El-Gayed, A., Shoeb, M. A., & Ahmed, M. M. (2020). Population dynamics of the vine mealybugs, *planococcus ficus* Signoret (Pseudococcidae: Homoptera) associated with grapevine in Fayoum governorate, Egypt. In Fayoum J. *Agric. Res. & Dev (Vol. 34*, Issue 2). doi: 10.21608/fjard.2020.189917

Tizro, P., Choi, C., & Khanlou, N. (2019). Sample Preparation for Transmission Electron Microscopy: Methods and Protocols. In *Methods in molecular biology* (Clifton, N.J.) (Vol. 1897, pp. 417–424). https://doi.org/10.1007/978-1-4939-8935-5_33

van Mierlo, J. T., Overheul, G. J., Obadia, B., van Cleef, K. W. R., Webster, C. L., Saleh, M. C., Obbard, D. J., & van Rij, R. P. (2014). Novel Drosophila Viruses Encode Host-Specific Suppressors of RNAi. *PLoS Pathogens, 10*(7). https://doi.org/10.1371/journal.ppat.1004256

van Til, N. P., Heutinck, K. M., van der Rijt, R., Paulusma, C. C., van Wijland, M., Markusic, D. M., Oude Elferink, R. P. J., & Seppen, J. (2008). Alteration of viral lipid composition by expression of the phospholipid floppase ABCB4 reduces HIV vector infectivity. *Retrovirology, 5*. https://doi.org/10.1186/1742-4690-5-14

Virgin, H. W. (2014). The virome in mammalian physiology and disease. *Cell, 157*(1), 142–150. https://doi.org/10.1016/j.cell.2014.02.032

Walker, P. J., Siddell, S. G., Lefkowitz, E. J., Mushegian, A. R., Adriaenssens, E. M., Alfenas-Zerbini, P., Dempsey, D. M., Dutilh, B. E., García, M. L., Curtis Hendrickson, R., Junglen, S., Krupovic, M., Kuhn, J. H., Lambert, A. J., Łobocka, M., Oksanen, H. M., Orton, R. J., Robertson, D. L., Rubino, L., … Zerbini, F. M. (2022). Recent changes to virus taxonomy ratified by the International Committee on Taxonomy of Viruses (2022). *Archives of Virology, 167*(11), 2429–2440. https://doi.org/10.1007/s00705-022-05516-5

Walton, V. M. & Pringle, K. L. 2004. Vine mealybug, Planococcus ficus (Signoret) (Hemiptera: Pseudococcidae), a key pest in South African vineyards. A review. South African *Journal of Enology & Viticulture, 25*(2):54-72. https://doi:10.21548/25-2-2140

Wang, Y., Burand, J. P., & Jehle, J. A. (2007). Nudivirus genomics: Diversity and classification. *Virologica Sinica, 22*(2), 128–136. https://doi.org/10.1007/s12250-007-0014-3

Waterworth, R. A., Wright, I. M., & Millar, J. G. (2011). Reproductive biology of three cosmopolitan mealybug (Hemiptera: Pseudococcidae) species, Pseudococcus longispinus, Pseudococcus viburni, and Planococcus ficus. *Annals of the Entomological Society of America, 104*(2), 249–260. https://doi.org/10.1603/AN10139

Wijesundara, Y. H., Herbert, F. C., Kumari, S., Howlett, T., Koirala, S., Trashi, O., Trashi, I., Al-Kharji, N. M., & Gassensmith, J. J. (2022). Rip it, stitch it, click it: A chemist's guide to VLP manipulation. *Virology, 577*, 105–123. https://doi.org/10.1016/j.virol.2022.10.008

Wine Folly. (2024). An overview of Mexican wine country. Wine Folly. Retrieved 20th of January 2025, from https://winefolly.com/deep-dive/an-overview-of-mexican-wine-country

Yu, X., Qiao, M., Atanasov, I., Hu, Z., Kato, T., Liang, T. J., & Zhou, Z. H. (2007). Cryo-electron microscopy and three-dimensional reconstructions of hepatitis C virus particles. *Virology, 367*(1), 126–134. https://doi.org/10.1016/j.virol.2007.05.038

Zell, R., Delwart, E., Gorbalenya, A. E., Hovi, T., King, A. M. Q., Knowles, N. J., Lindberg, A. M., Pallansch, M. A., Palmenberg, A. C., Reuter, G., Simmonds, P., Skern, T., Stanway, G., & Yamashita, T. (2017). ICTV virus taxonomy profile: Picornaviridae. *Journal of General Virology, 98*(10), 2421–2422. https://doi.org/10.1099/jgv.0.000911

Zhao, M., Dos Santos Tavares, C. P., & Schott, E. J. (2021). Diversity and classification of reoviruses in crustaceans: A proposal. J. Invertebr. *Pathol., 182*(107568), 107568. https://doi.org/10.1016/j.jip.2021.107568

Annex

Viral Particle Enrichment Protocol

Version 4. Authors: Miguel Angel Martínez Mercado and Marco Antonio Cisneros Vargas - Agricultural Virology Laboratory - CICESE

Date: September 18, 2023

Original Source: Luria N, et al. 2020 Isolation and characterization of a novel cripavirus, the first *Dicistroviridae* family member infecting the cotton mealybug *Phenacoccus solenopsis*. Archives of Virology https://doi.org/10.1007/s00705-020-04702-7

Materials and Reagents

1.5 mL tubes resistant to chloroform	TBE buffer pH 8.3
1.5 mL tubes not resistant to chloroform	Phosphate buffer 10mM pH 7.0
Microtube racks and 15 and 50 tubes	Chloroform:n-butanol (1:1, v/v)
Entomological forceps and spatulas for microtubes	10%, 15%, 20%, 25%, 30%, 35% and 40% Sucrose / TBE
PowerBeads Tubes (QIAGEN)	Mortar and pistil (Millex)
Ceramic beads 2.8 mm (brand)	0.8 µm PES Filter
Polypropylene 5 mL tubes (Beckman, REF326819)	15 mL Falcon tubes
0.45 µm PES Filter (Millex GP)	10 mL syringe
0.22 µm Filter (brand)	Ice

Equipment

Refrigerated centrifuge (HERMLE, Z 216 MK)
Optima MAX-XP Ultracentrifuge (Beckman)
MLS-50 Rotor (rav 71.7 mm) with sleeves (4 x 5mL) (Beckman)
Analytical balance

EDTA 0.5 M pH 8

Reagent	100 mL 1X
Sodium disodium EDTA	18.61 g
Water	80 ml
Adjust the pH with NaOH (in pellets)	

The EDTA will be dissolved by adding enough NaOH pellets (gradually).

Buffer TBE pH 8.3

Reagent	**1L 5X stock**	**100mL 5X**	**100mL 1X**
Tris base	54 g	5.4	1.08 g
Boric acid	27.5 g	2.75	0.55 g
EDTA 0.5 M pH 8	20 mL	10	2 mL
Adjust the pH			

Phosphate Buffer (PB) 0.01 M pH 7 (using heptahydrate)

Reagent	200 mL	100mL
Dibasic sodium phosphate heptahydrate (mw 268.07 g/mol)	309.75 mg	154.87 mg
Monobasic sodium phosphate monohydrate (mw 137.99 g/mol)	116.5 mg	58.27 mg
H2O	160 mL	80 mL
Adjust the pH and bring it to the final volume.		

Phosphate Buffer (PB) 0.01 M pH 7 (using anhydrous) Source: Link to source

Reagent	**for 100 mL, 0.01 M**	**dissolve in**	**Make up to**
Anhydrous dibasic sodium phosphate (142 g/mol)	142 mg	80 mL	100 mL
Monobasic sodium phosphate monohydrate (138 g/mol)	138 mg	80 mL	100 mL

	For pH 7, combine		
Dibasic	61 mL		
Monobasic	39 mL		

Day 1. Extraction, filtration and concentration.

NOTE: Solvents are used outside the fume hood in this stage. It is required to use a KN95 mask. Samples must be maintained at 4°C, always using ice.

1. Weigh 1 g of mealybugs, pour them into the mortar.

2. Add 2 ml of (1:1 v/v) TBE/PB buffer, proceed to macerate them adding an additional 2 ml when needed, once the sample has been macerated, use 2 additional ml of the TBE/PB buffer to clean the mortar and pistil, this will also be recovered. (Partial volume 6 mL).

3. Distribute the collected macerated 4 Eppendorf tubes.

4. Centrifuge the macerated sample for 10 min at 14,000 g at 4°C.

5. Collect the supernatant from all (4) tubes into a 15 ml tube (S1) and correctly label it, keep the tubes with the pellet (P1).

6. Add 600 µL TBE buffer and 60 µL of chloroform: n-butanol (1:1, v/v) to the tubes with the pellet.

7. Homogenize the sample using a vortex mixer for 20 seconds or until the sample is adequately uniform.

8. Centrifuge the sample for 10 min at 14,000 g at 4°C.

9. Collect the supernatant (S2) to a separate tube of 15 ml and correctly label it. (Discard pellet).

10. Filter S2 through a 0.45 µm PES filter. This process will be repeated for S1 adding a first filtering step using a 0.8 µm MCE membrane (Millex).

11. Maintain the samples on ice.

12. Record entry in the logbook, turn on the ultracentrifuge Optima Max XP (Beckman)

13. Clean the rotor MLS-50 and jackets (interior and exterior), verify the integrity of the rubber packings.

14. Set the ultracentrifugation to 160,000 x g for 3 H at a 4°C max acceleration and coast deceleration.

15. Distribute the S1 and S2 samples into the polypropylene centrifuge tubes (Beckeman) correctly labeling the tubes S1(tubes 1/3) and S2(tubes 2/4).

16. Match each tube to their corresponding jacket.

17. Adjust the weight on an analytic scale using TBE for each correspondent pair (tube 1 vs 3 and tube 2 vs 4) weight them including their tap and jacket.

18. Mount the jacket with the tube to their respective spot in the rotor, then carefully mount the rotor into the ultracentrifuge.

19. Start the centrifugation.

20. Once concluded carefully retrieve the jackets from the rotor and carefully recover the centrifugation tube.

21. The supernatant is discarded if each tube is discarded and 0.5 ml of PB is added to each tube.

22. Each tube is then covered with a parafilm membrane and stored overnight at 4°C.

Day 2 Separation.

1. Record entry in the logbook, turn on the ultracentrifuge Optima Max XP (Beckman).

2. Clean the rotor MLS-50 and jackets (interior and exterior), verify the integrity of the rubber packings.

Note: Gradient steps are made inside a cold room, therefore adequate clothing is required.

3. Carefully resuspend the pellet generated from the concentration with the aid of a 200 uL micropipette avoiding the generation of air bubbles.

4. The resuspended pellets from S1 (tubes 1/3) are combined into one tube and correctly labeled. The same process is repeated for the tubes of S2 (tubes 2/4).

5. Sucrose gradient

6. Select 4 polypropylene centrifuge tubes and correctly label them as S1 (tubes 1/3) and S2 (tubes 2/4).

7. Inside of the cold room add seven steps of 0.5 ml to each tube from bottom to top starting from 40% sucrose / TBE. The order of the steps is as follows: 40%, 35%, 30%, 25%, 20%, 15% and 10%.

8. Add 500 uL of the correspondent pellets to each tube either S1 or S2 and the position that the tube will take in the rotor from 1 to 4.

9. Allocate each tube with their correspondent jacket.

10. Measure the weight of the tubes with their jacket and their tap to adjust the weight on an analytic scale using TBE for each correspondent pair (tube 1 vs 3 and tube 2 vs 4) the weight of each pair must match up to thousands (example 50.111xx vs 50.111xx).

11. Load up the tubes into the ultracentrifuge each tube to their corresponding spot.

12. Ultracentrifuge at 100,000 x g, at 4°C during 2h (coast stop)

13. Once the centrifuge concludes, carefully unload the tubes and prop them side by side to take photographic evidence of the gradient formed.

14. Recover the formed gradient by taking 0.5 ml of the gradient until it has depleted; this will be allocated to 3 different 15 ml falcon tubes correctly label (tube 1 Top / tube 2 Middle / tube 3

Bottom) the tubes constitute the combination of fractions as following tube 1 fraction 1 and 2 (F1/F2) for top, tube 2 middle is the combination of the following fractions F3,F4,F5,F6 and F7.

15. The last fraction is left in each tube and 500 uL of PB buffer (filtered at 0.22 µm) is added, covered with parafilm membrane and stored overnight at 4°C.

Day 3/4/5 Sample cleaning.

Note: use ice to maintain samples at 4°C.

1. Resuspend the pellets stored overnight with the aid of a 200 uL micropipette.

2. Once the pellet is resuspended it is transferred together with the last fraction left overnight (fraction 8) to the 50 ml falcon tube label as tube 3 bottom.

3. PB buffer (0.22 uL filtered) will be added to each tube (Top/Middle/Bottom) until the total volume of each tube reaches 20 ml.

4. Note: the following steps (4-13) will be repeated for each tube (Top/Mid/Bot), this process may extend up to 3 days.

5. Distribute the 20 ml into four polypropylene centrifuge tubes, correctly label each tube and mount them into their respective sleeves.

6. Counterweight the tubes with their respective pair (tube 1 with tube 3 / tube 2 with tube 4) and sleeves using PB buffer.

7. Mount the weighted tubes into their respective spots in the rotor. Once the tubes are mounted carefully place the rotor into its spot on the ultracentrifuge.

8. Set the ultracentrifuge to 200,000 x g for 2 hours, with a cruising speed stop, at 4°C.

9. Once the centrifuge cycle is complete, recover the tubes and eliminate the supernatant.

10. Add 500 µl of PB buffer (0.22 uL filtered) to each tube, resuspend the pellet and add 4.5 ml of PB buffer (0.22 uL filtered).

11. Counterweight the tubes with their respective pair (tube 1 with tube 3 / tube 2 with tube 4) and sleeves using PB buffer.

12. Mount the weighted tubes into their respective spots in the rotor. Once the tubes are mounted carefully place the rotor into its spot on the ultracentrifuge. Set the ultracentrifuge to 200,000 x g for 2 hours, with a cruising speed stop, at 4°C.

13. Once the centrifugation cycle is complete the supernatant is discarded and 50 uL of PB buffer (0.22 uL filtered) is added to the pellet, the lid is covered with parafilm membrane and stored overnight with ice.

Day 6

1. The pellets will be resuspended and combined with their respective partners into an eppendorf correctly labeled as VLPX (X refers to the number of VLP it corresponds to) and the position of the fractions that it contains (Top/Mid/Bot).